Klara Lanz, BSc.

Characterization of potentially pathogenic *Vibrio* spp. via Raman Spectroscopy

MASTER'S THESIS

to achieve the university degree of

Master of Science

Master's degree programme: Molecular Microbiology

submitted to

Graz University of Technology

Supervisor

Assoc.Prof. Dipl.-Ing. Dr.techn. Harald Pichler

Institute of Molecular Biotechnology, Graz University of Technology

Host Supervisor Dr. Gunnar Gerdts
Microbial Ecology
Biological Institute Helgoland, Alfred Wegener Institute

Graz, August 2017

AFFIDAVIT

I declare that I have authored this thesis independently, that I have not used other than the declared sources/resources, and that I have explicitly indicated all material which has been quoted either literally or by content from the sources used. The text document uploaded to TUGRAZonline is identical to the present master‘s thesis.

_____	_____
Date	Signature

Inhalt

Abstract

Bacteria of the genus *Vibrio* naturally occur in marine habitats and while some species live in symbiosis with marine organisms, others are considered as human pathogens. Increasing numbers of infections caused especially by the species *V. cholerae*, *V. parahaemolyticus* and *V. vulnificus,* have been correlated to rising sea water temperatures. Due to climate change, further temperature increases are expected and to understand the resulting changes in the environmental *Vibrio* population, fast and reliable detection and identification methods are required. During the present study, Raman spectroscopy was evaluated as identification method for potentially pathogenic *Vibrio* spp. For this purpose, five potentially pathogenic *Vibrio* spp. were chosen from the internal strain collection of the BMBF project VibrioNet and analysed using the Bio Particle Explorer. The Bio Particle Explorer combines a Raman spectroscope with a fluorescence microscope to achieve a high spatial resolution of about 1 µm. In order to perform automatic measurements, parameters for the optical image analysis, the correct cell recognition and selection were established. Furthermore, a practical way of sample preparation was established by testing different sample carriers, cell concentrations and fluorescent dyes. The strains were cultivated in alkaline peptone water and analysed spectroscopically in three independent batches. The acquired spectra were pre-processed in two ways and examined statistically for differences between the species. In the permutational multivariate analysis of variance (PERMANOVA) significant differences between the species were detected. Additionally, a support vector machine was trained and cross-validation confirmed a high separability of the species. The combination of Raman spectroscopy and statistical analyses allowed a differentiation of *Vibrio* strains on species level although the methodology still needs to be adapted for environmental isolates.

1. Introduction

1.1. Raman spectroscopy

When light strikes matter, it might interact with its atoms or molecules in different ways. The light beam can be reflected, absorbed, transmitted or scattered. In Fourier-Transform-infrared spectroscopy the infrared light excites molecular vibrations and gets thereby absorbed by the sample. This absorbance leads to substance specific spectra which can be compared to reference spectra for identification. The scattering of light is based on vibrational, rotational, and other low-frequency interactions with the sample and occurs in two ways (Long, 2002). Most of the incident photons are elastically scattered and undergo no change in their wavelength λ which was first described by Lord Rayleigh in 1871 (Hollas, 2004). Only about one millionth part of the scattered light is inelastically scattered, whereby the light either gains or loses energy. Through this shift in wavelength, the so-called Raman shift, additional bands appear left and right of the Rayleigh band and together form the specific spectrum of the analysed substance (Figure 1).

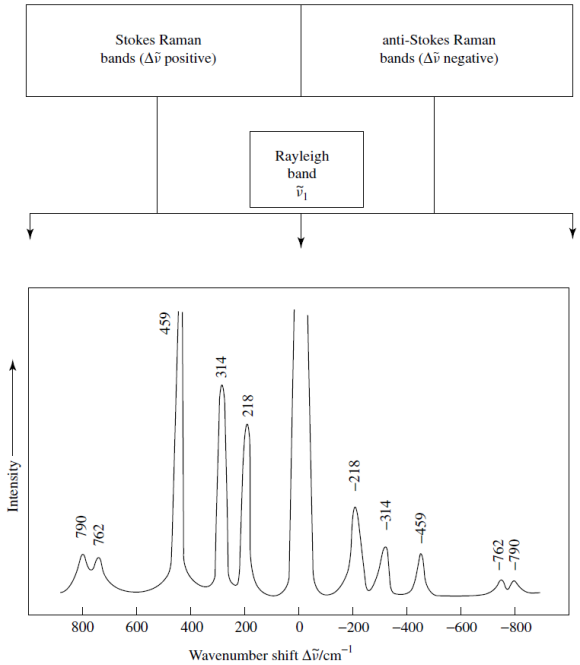

Figure 1: Spectrum of carbon tetrachloride. The Rayleigh band is flanked by the Raman bands that originate from photons which either lost energy (Stokes bands) or gained energy (Anti-Stokes bands) during the scattering process. As only the Stokes bands are analysed in this study the abscissa is labelled as wavenumber/cm^{-1} and the values decrease from left to right. (Long, 2002)

Stokes bands originate from photons that lost energy through colliding with and exciting vibrations in molecules. Anti-Stokes bands arise from photons which gained energy during the scattering process. The vibrating molecules must be in an excited state to be able to transfer energy to the photons but since most molecules are in the ground state at room temperature these transitions are less likely to happen. For that reason, the anti-Stokes bands are less intense and it is common to use only the more intense Stokes bands in Raman spectroscopy.

The change in wavelength is depicted as wavenumber $\tilde{\nu} = \frac{1}{\lambda}$ [cm^{-1}] which equals the number of sine waves per cm (Otto, 2006). The phenomenon of inelastically scattered light was first postulated in 1923 by the Austrian theoretical physicist Smekal (Smekal, 1923) and five years later practically demonstrated by the Indian physicist Raman and his collaborator Krishnan (Long, 2002; Smith and Dent, 2005). For the original experiment, a telescope was used to focus sunlight onto a purified liquid or dust-free vapour. Optical filters were used to collect and detect the scattered radiation (Raman and Krishnan, 1928). Depending on the scientific question, modern Raman spectrometer use lasers either in ultraviolet (e.g. 244 nm), visible (e.g. 532 nm) or near infrared (e.g. 785 nm) wavelengths.

Raman and infrared spectroscopy are comparable but complementary techniques based on molecular vibrations. While infrared light activates vibrational modes through a change in the dipole moment of a molecule, Raman spectroscopy changes its polarization. Molecules with one centre of symmetry underlie the rule of mutual exclusion and, therefore, can either be infrared or Raman active. In polyatomic molecules, the vibrations arise from more than just one bond and are more complicated to interpret. Theoretically, calculated bands can vary in a recorded spectrum due to overlays or degenerations of vibrations (Otto, 2006). Biological samples consist mostly of water and are usually prepared in aqueous solution. As while water has strong absorbing properties the polarizability can hardly be changed. Therefore, the major advantage of Raman over infrared spectroscopy is that water gives only weak Raman signals and does not interfere with signals originating from the sample itself. This saves time during sample preparation, as samples do not have to be dried over a long period. Different bacterial cells consist of the same molecules and building blocks, but with different abundance of these molecules (amino acids, nucleotides, lipids, etc.). Just as the chemical composition differs between bacterial species so do the bands in the Raman spectra differ in their presence and intensity. In bacterial spectra, the bands appear in two major regions, the fingerprint region (585 cm^{-1} - 1750 cm^{-1}) and the CH-stretch region (2800 cm^{-1} - 3050 cm^{-1}) which are separated through a silent region. These two spectral regions can either be used together or separately in the analysis of the data.

1.2. *Vibrio*

Vibrio are gram-negative, rod-shaped, facultative anaerobic, oxidase and catalase positive bacteria belonging to the class of *Gammaproteobacteria*. They can be found in aquatic habitats such as sediments, estuaries and marine coastal waters and live as planktonic cells as well as attached to surfaces of living organisms or marine debris (Barbieri et al., 1999; Thompson et al., 2004; Farmer et al., 2005; Kirstein et al., 2016). Some *Vibrio* live in symbiosis with marine organisms; others can be pathogenic to human or cause zoonoses. *Vibrio cholerae*, *Vibrio parahaemolyticus* and *Vibrio vulnificus* are counted as higher risk organisms which can cause severe infections and diseases like diarrhoea, gastroenteritis, wound infections and septicaemia via ingestion or contact with contaminated water (Austin, 2010; Thompson et al., 2004). The lower risk organisms *Vibrio alginolyticus* and *Vibrio mimicus* can be the cause of ear infections or gastroenteritis, respectively (Hornstrup and Gahrn-Hansen, 1993; Takahashi et al., 2007). *Vibrio* infections are common, for example in tropical zones.

However, during the last decade increasing numbers of infections were documented in European coastal regions of the Mediterranean Sea as well as the Baltic Sea (Martinez-Urtaza et al., 2005; Eiler et al., 2006). Observations have shown that rising sea surface temperatures favour the growth of *Vibrio* spp. and correspond with rising numbers in *Vibrio* infections (Baker-Austin et al., 2010; Baker-Austin et al., 2012; Oberbeckmann et al., 2011a). Due to climate change a further increase of water temperatures in the North and Baltic Sea is expected. In order to estimate resulting changes in environmental *Vibrio* populations and the potential risk of increasing numbers of infections, fast and specific identification methods are needed. In recent studies, molecular methods such as PCR (Oberbeckmann et al., 2011b) or Matrix Assisted Laser Desorption/Ionization - Time of Flight Mass Spectrometry (MALDI-TOF MS) (Erler et al., 2015) are used for species-specific identifications of environmental *Vibrio*. Those methods are partly culture-dependent, time-consuming or require large amounts of cell material to classify and identify bacterial species (Hlaing et al., 2016). Raman spectroscopy, however, is a culture-independent method and has been established in microbiological research over the last years (Stöckel et al., 2016). The combination of Raman spectroscopy and light microscopy results in a high spatial resolution of about 1 µm (Harz et al., 2009). Clear advantages of this micro-Raman spectroscopy are the small amount of cell material required to gather single cell spectra (Huang et al., 2004) and the possibility of mixed culture analysis (Hlaing et al., 2016).
Medically relevant microorganisms such as *Escherichia coli*, *Pseudomonas spp., Listeria spp.* as well as *Staphylococcus* spp. have successfully been differentiated via Raman spectroscopy (Kusic et al., 2015; Harz et al., 2005; Meisel et al., 2014).In the course of this thesis, Raman spectroscopy was evaluated as identification method for potentially pathogenic *Vibrios* on species level.

1.3. Aims of this thesis

The aim of this study was to evaluate Raman spectroscopy as a quick and sensitive screening and identification method for potentially pathogenic *Vibrios* on species level. To increase efficiency, the Bio Particle Explorer, a combination of a microscope and Raman spectrometer, may be used in an automatic mode, whereby it chooses and analyses samples according to tuneable parameters.
Specific aims:

- Establishing a practical way of sample preparation, tailored to the different requirements of the samples and the equipment.
- Establishing the parameters for the automatic Raman analysis to enable a correct particle recognition, detection and measurement.
- Determining which parts of the recorded spectra should be used in the statistical analyses to successfully identify the *Vibrio* spp.

2. Materials and methods

2.1. Bio Particle Explorer

The Bio Particle Explorer (BPE 118-100 200416, rap.ID Particle Systems GmbH, Berlin, Germany) combines a Raman spectroscope and fluorescence microscope. The microscope (BX41M-LED, Olympus) was equipped with a 100x objective (NA = 0.9, MPLFLN, Olympus) and, in combination with different filters, was used in bright field, dark field or fluorescent mode. The light source was a LED lamp (M470L3-C1, Thorlabs) with a nominal wavelength of 470 nm. In the fluorescent mode, a band-pass excitation filter (475/35 nm, FF01-475/35-25, Semrock) combined with a dichroic beamsplitter (488 nm, DI02-R488-25x36, Semrock) and a band-pass emission filter (530/43 nm, FF01-530/43-25, Semrock) was used. The optical analysis of samples was performed with a charged-coupled device (CCD) camera (Stingray F-145B, Allied Vision Technologies). Size parameters and positions of bacteria were automatically recorded by the system using the software Accu (version 3.1.6.7, rap.ID Particle Systems GmbH). Particle parameters, such as size and elongation, served as selection parameters for automatic Raman measurements. For Raman spectroscopy, a diode-pumped solid-state (DPSS) frequency doubled Nd:YAG Laser (Samba™, Cobolt) with a wavelength of 532 nm was focused onto the sample with 7.5 mW or 15.75 mW intensity. During the total exposure time of 20 s two spectra of 10 s each were recorded for spike removal (see 2.6.1). The backscattered Raman light was diffracted by a single-stage monochromator (HE 532, Horiba) and detected by a thermoelectrically cooled back-illuminated CCD camera (DV104A-BV, Andor Technologies) with a spectral resolution of approximately 6 cm^{-1}. The spectra of single cells were collected in a range from 200 cm^{-1} to 3200 cm^{-1}. The BPE detects cells with automatic image analysis, either by reflected dark field microscopy or by fluorescence microscopy. In reflected dark field microscopy the incident light illuminating the specimen from above is reflected, refracted or diffracted by the specimen, re-enters the objective and is then detected by the CCD camera (Figure 2).

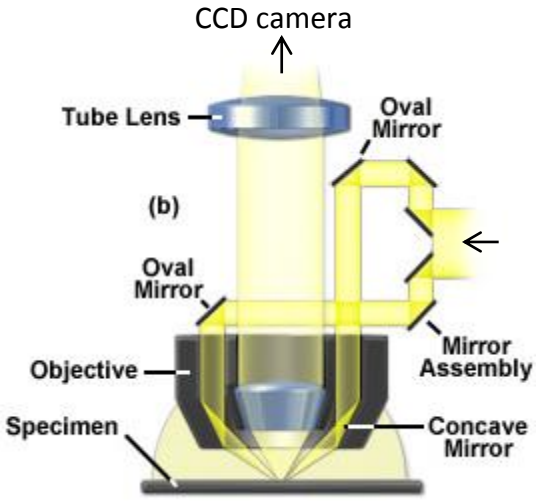

Figure 2: Principle of reflected dark field microscopy. (modified from Rottenfusser et al. (2014))

This way of contrasting can be used with smooth sample carriers, foil for example, because it uses the three-dimensionality of the sample to differentiate it from the background. The rays of light hitting the smooth sample carrier are reflected as well but miss the objective and, therefore, these positions appear black. When using sample carriers with uneven surfaces, like filters, the principle of dark field microscopy cannot differentiate correctly between sample and background. Therefore, in these cases the automatic analysis of cells can only be performed using fluorescence microscopy. Consequently, the cells have to be stained to receive only signals from the sample. In Raman spectroscopy, it is important to use a fluorescent dye that cannot be excited by the Raman laser (532 nm).

2.2. Bacterial strains and cultivation

The *Vibrio* strains originated from the internal strain collection of the BMBF project VibrioNet, stored in the Microbank System in liquid nitrogen. These strains were isolated from surface water samples at different locations of the North and Baltic Sea (Erler et al., 2015; Kirstein et al., 2016). At the beginning of this thesis, two strains per species were reactivated. To verify the species identities MALDI-TOF MS was performed and one stain per species was chosen for the following work (Table 1). During MALDI-TOF MS, one strain (VN-4234), formerly classified as *V. cholerae* could be identified as *V. mimicus*. This strain was excluded from Raman measurements and will only be discussed in the MALDI-TOF MS sections.
For the reactivation, 10 mL of sterile alkaline peptone water (APW, Merck KGaA, Darmstadt, Germany) were inoculated with one bead from the Microbank stock culture. APW is a culture medium used for the selective enrichment of *Vibrio*. The concentration of 2 % sodium chloride favours the growth of *Vibrio* spp. and, combined with the alkalinity of pH 8.5, inhibits most unwanted growth of other bacteria. The cultures were incubated at 18°C and 18 rpm, to enable a slow adaption, and after 6 h were shifted to 37°C for further incubation overnight.

Table 1. *Vibrio* strains. *V. alginolyticus* VN-2655, *V. cholerae* VN-4241 *V. vulnificus* VN-4256 *V. mimicus* VN- 4254 *V. parahaemolyticus* VN-2992 were chosen for the characterization via Raman spectroscopy.

Species	VibrioNet-strain	Sampling location
V. alginolyticus	VN-2655	North Sea
V. cholerae	VN-4241	Baltic Sea
V. vulnificus	VN-4256	North Sea
V. mimicus	VN-4254	North Sea
V. parahaemolyticus	VN-2992	North Sea

Differential streaking was performed on marine broth (MB) agar (Oppenheimer and ZoBell, 1952) with a reduced salinity of 50 % (MB-50 % = 16 PSU) using 1 µL inoculation loops. The plates were incubated at 37°C for 16-18 h and, afterwards, the cultures were stored at 18°C. Every two weeks, the strains were transferred to fresh MB-50 % agar plates and incubated as described above. For overnight cultures, single colonies were picked from the stored agar plates with 1 µL inoculation loops suspended in 10 mL sterile APW and incubated at 37°C and 18 rpm overnight or for 17 h, for preliminary experiments or Raman Spectroscopy,

respectively. The optical cell density (OD_{600nm}) of the overnight cultures was determined using a photometer (BioPhotometer, Eppendorf, Hamburg, Germany) and was used to calculate the cell number/mL using the linear regression equation [1] of *V. cholerae*. The equation was provided by Sidika Hackbusch, MSc.

$$\frac{cells}{mL} = \frac{OD_{600nm} - 5.62 * 10^{-3}}{3.9 * 10^{-10}} \quad [1]$$

E. coli DSMZ-1576 (Deutsche Sammlung von Mikroorganismen und Zellkulturen, Braunschweig, Germany) was cultivated and provided by Sidika Hackbusch, MSc. The strain was only used as positive control for the fluorescent staining with CFDA-SE (see 2.4.1).

2.3. MALDI-TOF MS

Matrix Assisted Laser Desorption/Ionization - Time of Flight Mass Spectrometry (MALDI-TOF MS) was used to verify the species identity of the used strains. This spectrometric technique uses a soft ionization and allows a fast analysis of biomolecules through their mass-to-charge-ratio. As the cells analysed via MALDI-TOF MS have to be fresh, single colonies were transferred to MB-50 % agar plates and incubated as mentioned above (2.2) for less than 24 h before the measurement. Then, colonies were picked with a sterile toothpick and, in triplicates, transferred homogeneously on a MALDI-TOF MS target plate (MSP 96 target polished steel) in a thin layer. The samples were overlaid with 1 µL of 70 % (v/v) formic acid to break the cells and, after the fluid had dried up, covered with 1 µL of matrix solution (saturated solution of α-cyano-4-hydroxycinnamic acid in 50 % acetonitrile and 2.5 % trifluoroacetic acid) according to the manufacturer's manual (Bruker Daltonics Inc., Bremen, Germany). The samples were analysed in a microflex LT/SH system (Bruker Daltonics Inc., Bremen, Germany) in linear mode. The measurement parameters are listed in Table 2. The acquired mass spectra were analysed, using the Biotyper™ RealTimeClassification software (version 3.1), by comparing them to the Bruker library and the internal VibrioBase Library (Erler et al., 2015). For a secure genus and probable species identification, a score value above 2.0 is required. Score values higher than 2.3 indicate highly probable species identifications (Erler et al., 2015).

Table 2. MALDI-TOF MS measurement parameters.

Ion source	20 kV
Lens	3 kV
Laser frequency	60 Hz
Sample rate	0.5 GS/s
Detection mass range	2600 – 20000 Da
Detector gain	9.5x 2842 V

2.4. Establishing sample preparation

2.4.1. Fluorescence microscopy

For single cell measurements, micro-Raman spectroscopy requires a high magnification, wherefore the BPE is equipped with a 100x objective. Fluorescence microscopy was performed to receive a more general overview during preliminary experiments. It was used to determine which cell concentration should be used in order to achieve a good distribution of cells, to examine the results of the fluorescence staining with two different fluorescent dyes and to check the usability of a metal array which is intended to allow optimal use of the filter surface.

Fluorescence microscopy was carried out with an optical microscope (Axioplan 2 imaging, Zeiss, Oberkochen, Germany) using the software AxioVision 32 bit 4.8.2 SP 3 (Zeiss, Oberkochen, Germany). The microscope was equipped with a halogen lamp (HAL 100) and a mercury arc lamp (HBO 100). To detect green fluorescent cells, stained with SYBR Green I (Sigma-Aldrich, St. Louis, USA), Carboxyfluorescein diacetate succinimidyl ester (CFDA SE, Molecular Probes, Eugene, USA) or SYTO 9 (Molecular Probes, Carlsbad, USA) the filter set 09 (Olympus, Shinjuku, Japan) was used. This filter set consists of a band-pass excitation filter (BP 450 – 490 nm), a long-pass emission filter (LP 515 nm) and a dichroic mirror as beamsplitter (FT 510 nm). All dyes and stained samples were protected from light to prevent fading. The fluorescent dye parameters are summarized in Table 3.

Table 3. Fluorescent dye parameters. To reduce the side effects of fluorescence within the Raman spectra only fluorescent dyes which cannot be excited by the Raman laser should be used.

Name	Excitation [nm]	Emission [nm]	Colour	concentration
SYBR Green I	497	520	Green	1x
CFDA SE	492	517	Green	1 µM
SYTO 9	480	500	Green	0.12 µM

Cell concentration determination

V. alginolyticus VN-2655 cells were harvested by centrifugation (13,000 rpm, 5 min) and washed two-times with 1x PBS. They were fixed with 0.75 % (w/v) formaldehyde for 45 min and stained with 1x SYBR Green I for 18-20 min at room temperature in the dark (Patel et al., 2007). SYBR Green I is a fluorescent dye that preferentially binds double-stranded DNA but also stains single-stranded DNA and RNA. SYBR Green I stains living and dead cells. To prevent the cells from clumping, the suspension was vortexed for 20-30 s after each step. Cell suspensions with different cell concentrations ($1x10^6$, $5x10^6$, $1x10^7$, $1x10^8$ and $1x10^9$ cells/mL) of the stained *V. alginolyticus* were filtered onto Polycarbonate filters with a pore size of 0.2 µm (GTTP, Isopore™ membrane filter, Merck, KGaA, Darmstadt, Germany) using an 8 µm cellulose nitrate filter (Sartorius AG, Göttingen, Germany) as backing filter. After drying, the filters were mounted to glass slides (Menzel glasses, Thermo Fisher Scientific, Braunschweig, Germany) with a 0.1 % p-phenylenediamine anti fade medium and analysed by fluorescence microscopy with 1000x magnification. Cells were counted on 12 images taken on four

independent 0.2 µm GTTP filters using the software ImageJ2x (Rasband, 1997-2016) and the average cell number/mm^2 was calculated.

Fluorescent dyes for Raman spectroscopy

Fluorescent dyes excited by the Raman laser would cause interferences between the fluorescence signal and the Raman spectrum of the sample. Other than SYBR Green I, Carboxyfluorescein diacetate succinimidyl ester and SYTO 9 are fluorescent dyes that have previously been used with Raman spectroscopy. Krause et al. (2007) showed that these two dyes had no significant influence on the Raman spectra of stained bacteria and were therefore used in this study. Read and Whiteley (2015) published that 2 % (w/v) of formaldehyde can be used for Raman spectroscopy without having an influence in the bacterial spectra. To ensure a complete fixation of the potentially pathogenic *Vibrio* the previously used concentration of 0.75 % (w/v) formaldehyde was adapted to 2 % (w/v) while the other steps of fixation stayed the same.

Carboxyfluorescein diacetate succinimidyl ester (CFDA SE) is a colourless non-fluorescent vital stain which passively diffuses into cells. Its diacetate groups are cleaved by intracellular esterases in living cells. The succinimidyl ester group forms fluorescent conjugates with intracellular amines that are well retained within the cells. With the fluorescence excitation maximum at 492 nm, the dye should not interfere with the Raman signal of the sample. The staining was performed as recommended by the manufacturer (Molecular Probes, Eugene, USA) with 1x10^7 cells of *V. alginolyticus*. The fixation was performed afterwards as mentioned above. SYTO 9 is a green fluorescent nucleic acid stain that can be used to stain living as well as dead cells. It is cell permeant and stains DNA as well as RNA. With a distance of 52 nm, the excitation maximum of SYTO 9 lies furthest apart from the Raman laser wavelength (532 nm). The staining was performed as recommended by the manufacturer (Molecular Probes, Carlsbad, USA) after the fixation of 5x10^6 cells of *V. alginolyticus*.

Metal array

As it is not necessary for Raman spectroscopy to analyse large filter areas covered with cells, a metal array was internally designed to fit the filtration device to apply 12 samples per filter in parallel. From the top of the array the holes are cylindrical with a diameter of 1 mm and widen conically on the bottom side to a diameter of 1.4 mm (Figure 3). It was used in the upright orientation and upside down, to see whether the shape of the holes lead to different results when filtering cells onto a 0.2 µm GTTP filter. Drops of 1 µL containing 1x10^6, formaldehyde fixed and SYBR Green I (see 2.4.1) stained, *V. alginolyticus* cells were pipetted into each hole while a vacuum pump applied a negative pressure of 200 - 600 mbar.

The array was tested with or without an 8 µm cellulose nitrate backing filter (Sartorius AG, Göttingen, Germany), and with or without Parafilm M® (Bemis, Neenah, USA) used to tighten up the filtration unit.

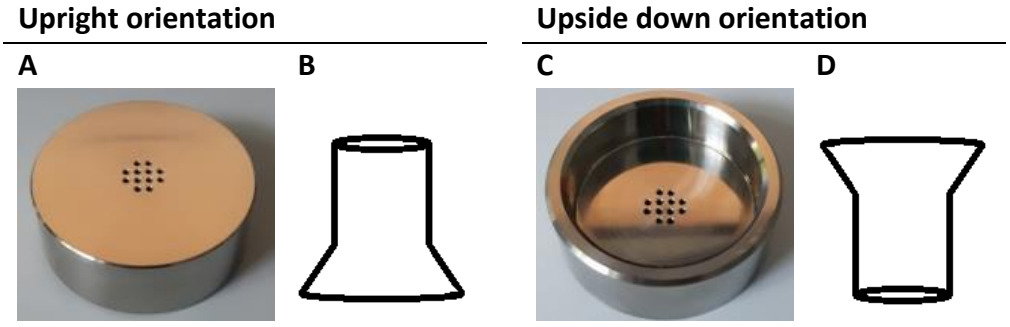

Figure 3: Photographs of the metal array. In the upright orientation (A) the holes open up conically at the bottom (B). The metal array was also used upside down (C) to see whether this orientation of the holes (D) improved the filtration result.

2.4.2. Nickel slit filters and silver membrane filters

It is necessary to use filters made of Raman inactive materials such as nickel or silver to detect only spectral information of the samples. In this study nickel slit filters (0.3-0.4 µm, rap.ID, Berlin, Germany) and silver membrane filters (0.2 µm, Pieper Filters, Bad Zwickenahn, Germany), both with a diameter of 13 mm, were tested. A glass filtration unit for 13 mm diametric filters was used with or without an 8 µm cellulose nitrate backing filter. The filtration unit had to be tightened with Parafilm around the junction between the funnel and the glass frit.

2.4.3. Nickel foil

Cells were fixed as mentioned in the section "Fluorescent dyes for Raman spectroscopy" (2.4.1) but not stained, as this was not necessary for this type of sample carrier. To remove extracellular substances and media components, the cells were harvested by centrifugation at 11,000 rpm for 5 min. The supernatant was removed, the cells were resuspended in 1 mL MQ H_2O and mixed by vortexing. Drops of the cell suspensions were spotted onto the foil, incubated for 5 min and taken off afterwards. To receive an appropriate number of cells to perform automatic single cell measurements, combinations of different drop volumes (3 – 20 µL) and cell concentrations ($1x10^6$ – $1x10^9$ cells/mL) were tested. For wavenumber calibration, few acetaminophen (APAP) grains were transferred to the nickel foil with a sterile toothpick. The completely dried foils were taken to the BPE and the Raman measurements were performed in dark field mode.

2.5. Particle recognition and automatic selection

For the particle recognition, greyscale images were recorded and binarized. In these greyscale images cells contrast from the black background as bright signals. A binarization threshold was set, which was then used on the whole image to detect the cell signals and convert the images to "grey" (signal) and "white" (background). The grey areas in the image were then counted

as particles and their size parameters were measured. If the threshold is set too low only fragments of the particles are detected and if it is too high particles lying close together cannot be distinguished as separate particles. As the images were 8-bit images the threshold could be fixed to a greyscale value from 0 (black) to 255 (white). To determine which threshold value enabled the best particle recognition for *Vibrio* cells, an area of 4-fields was measured with values between 200 and 240 (Δ10 units). Before the automatic Raman measurements were performed, the manual mode was used to find which size parameters should be selected for the different species to exclude artefacts like cell groups and particle fragments from the analysis. Another important requirement for a correct particle recognition as well as a correct spectroscopic measurement was finding the right focus. For an overview image, the focus was adjusted manually. To ensure that the Raman measurements were performed correctly during automatic measurements, an autofocus was performed on each selected particle beforehand.

2.6. Characterization of *Vibrio* spp. via Raman spectroscopy

The automatic measurements, which lead to the results for the characterization of *Vibrio* species, were performed in dark field mode and on nickel foil. Five *Vibrio* strains (Table 1) were analysed in three independent batches per species. For one batch, an automatic measurement was performed for over 100 cells. From the acquired spectra, 50 - 100 spectra were chosen for the statistical analysis. Spectra with peaks visible in the silent region or low counts (Raman intensities) in the CH-stretch region were manually excluded from the data analysis.

2.6.1. Statistical analysis

Raw Raman spectra consist of signals originating not only from the sample but from various side effects (Figure 4), which have to be corrected before further statistical analyses are performed.

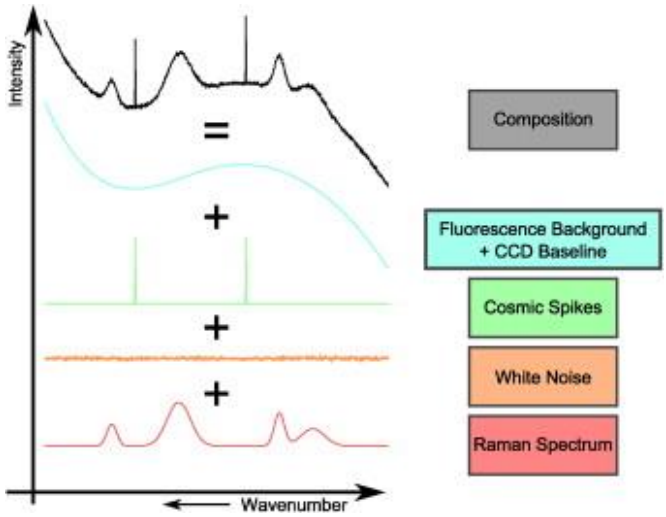

Figure 4: Composition of a Raman spectrum. Not all information included in raw Raman spectra originates from the sample itself. These side effects need to be corrected before the statistical analysis of the data. (Bocklitz et al., 2011)

High background signals either arise from the CCD camera's baseline or from auto fluorescence of the sample. Cosmic spikes occur when high energy particles hit the CCD camera and consequently can be seen as single events with high Raman intensity. Uncorrelated processes lead to Gaussian distributed noise. The raw Raman spectra were recorded from 200 cm^{-1} - 3200 cm^{-1} but could be truncated to the wavenumbers 585 cm^{-1} - 3100 cm^{-1} to exclude notch filter artefacts. The silent region (1800 cm^{-1} - 2680 cm^{-1}) was removed to further decrease the computational costs.
In this study, two different statistical approaches were applied on the data set. A support vector machine (SVM) and multivariate analysis (PCoA, PERMANOVA). SVM is a class modelling technique, that learns significant differences between groups. The raw data set was pre-processed and pre-treated according to Bocklitz et al. (2011). Cosmic spikes were corrected by a comparison of the two raw spectra, which got recorded for each selected particle. For wavenumber calibration, 20 bands of APAP spectra were used with a polynomial degree of 3 (Dörfer et al., 2011). Background correction was performed by the SNIP algorithm (Ryan et al., 1988), with iteration 30.
This pre-processed data set was used for the support vector machine and multivariate analysis. The SVM compares the labelled classes in pairs and creates a model where these classes get separated by a linear decision value. After combining all different comparisons, the model can be used to classify and identify unknown spectra. For comparison, another data set was taken from the SPE Reports to perform multivariate analysis. It consists of spectra originating from the same single cell measurements but it was spike and background corrected by the manufacturer's software, ACCU (rap.ID). No wavenumber calibration was performed. Truncation of the spectra was performed manually.

Before analysing the spectra with permutational multivariate analysis of variance (PERMANOVA) all data was square root transformed and Bray-Curtis similarity matrixes were calculated using Primer 6+ (PRIMER-E, Plymouth, UK). One-way tests were performed with unrestricted permutations of raw data. Two-way tests of the factors "species" and "batch" and one-way pair-wise *a posteriori* comparisons of the factor "species" were performed, with permutation of residuals, under a reduced model. Pair-wise *a posteriori* comparisons of the factor "species" were performed using unrestricted permutations of the raw data. All PERMANOVA tests were performed using 999 permutations and a significant difference was defined as $p(perm) > 0.05$. Further tests, like the similarity percentage analysis (SIMPER) and the clustering of group centroids, were performed to determine which parts of the spectrum contribute most to the differences between the species.

3. Results

3.1. Bacterial strains and cultivation

The optical density of the overnight cultures was measured and used to calculate the cell concentration per mL (Table 4). During the 17 h incubation, the *Vibrio* strains grew to cell densities between 9.55x10^8 cell/mL (*V. cholerae*) and 1.39x10^9 cell/mL (*V. parahaemolyticus*).

Table 4. Average cell density of overnight cultures grown in APW after 17 h incubation.

Species	VibrioNet-strain	OD_{600nm}	cells/mL
V. alginolyticus	VN-2655	0.445	1.13 x10^9
V. cholerae	VN-4241	0.386	9.76 x10^8
V. mimicus	VN-4254	0.378	9.55 x10^8
V. parahaemolyticus	VN-2992	0.547	1.39 x10^9
V. vulnificus	VN-4256	0.446	1.13 x10^9

3.2. MALDI-TOF MS

For the strains, *V. mimicus* VN- 4254, *V. parahaemolyticus* VN-2992 and *V. vulnificus* VN-4256, the species was verified with a high probability on species level with average score values higher than 2.3. With an average score value of 2.29 the species identification of *V. alginolyticus* VN-2655 was probable and accepted as verification of the species. The strain VN-4241 was identified as *V. cholerae* with a high probability on species level with an average score value of 2.36, however it was worth mentioning that the standard deviation of 0.15 was the highest observed (Table 5).

Table 5. MALDI-TOF MS verification of *Vibrio* species. The average score values and the corresponding standard deviations (SD) were calculated from three measurements.

Species	VibrioNet-strain	Species identification	Score Value	SD
V. alginolyticus	VN-2655	*V. alginolyticus*	2.29	0.03
V. cholerae	VN-4241	*V. cholerae*	2.36	0.15
V. mimicus	VN- 4254	*V. mimicus*	2.48	0.03
V. parahaemolyticus	VN-2992	*V. parahaemolyticus*	2.49	0.07
V. vulnificus	VN-4256	*V. vulnificus*	2.46	0.01

In previous work the *Vibrio* strain VN-4234 had been classified as *V. cholerae* but the MALDI-TOF MS measurement identified it as a *V. mimicus* (average score value of 2.44±0.05).

3.3. Fluorescence microscopy

3.3.1. Cell concentration determination

In order to detect single, well distributed cells on filters, various cell concentrations were concentrated on GTTP filters and stained with SYBR Green I (Figure 5). Fluorescence microscopy images showed that samples with $1x10^8$ or $1x10^9$ cells/mL were too concentrated for the visualization of single cells on the filter area. The cells formed large groups or a dens filter cake. With the lower concentration of $1x10^7$ cells/mL single cells could be visualized but small clusters of approx. 10 cells were still detectable. At a concentration of $5x10^6$ cells/mL, most cells were spread in the desired distribution. Hardly any single cells could be found in the middle of the filtration area, only around the edges in larger groups (picture not shown) at the concentration of $1x10^6$ cells/mL. Therefore, the concentration of $5x10^6$ cells/mL was chosen to determine the average cell number/mm^2 that was found inside the filtration area. Counting the cells inside the field of view on 12 independent micrographs led to an average number of 9066 cells/mm^2. Higher numbers of cells clustered at the edges of this area, but were not included in the calculations.

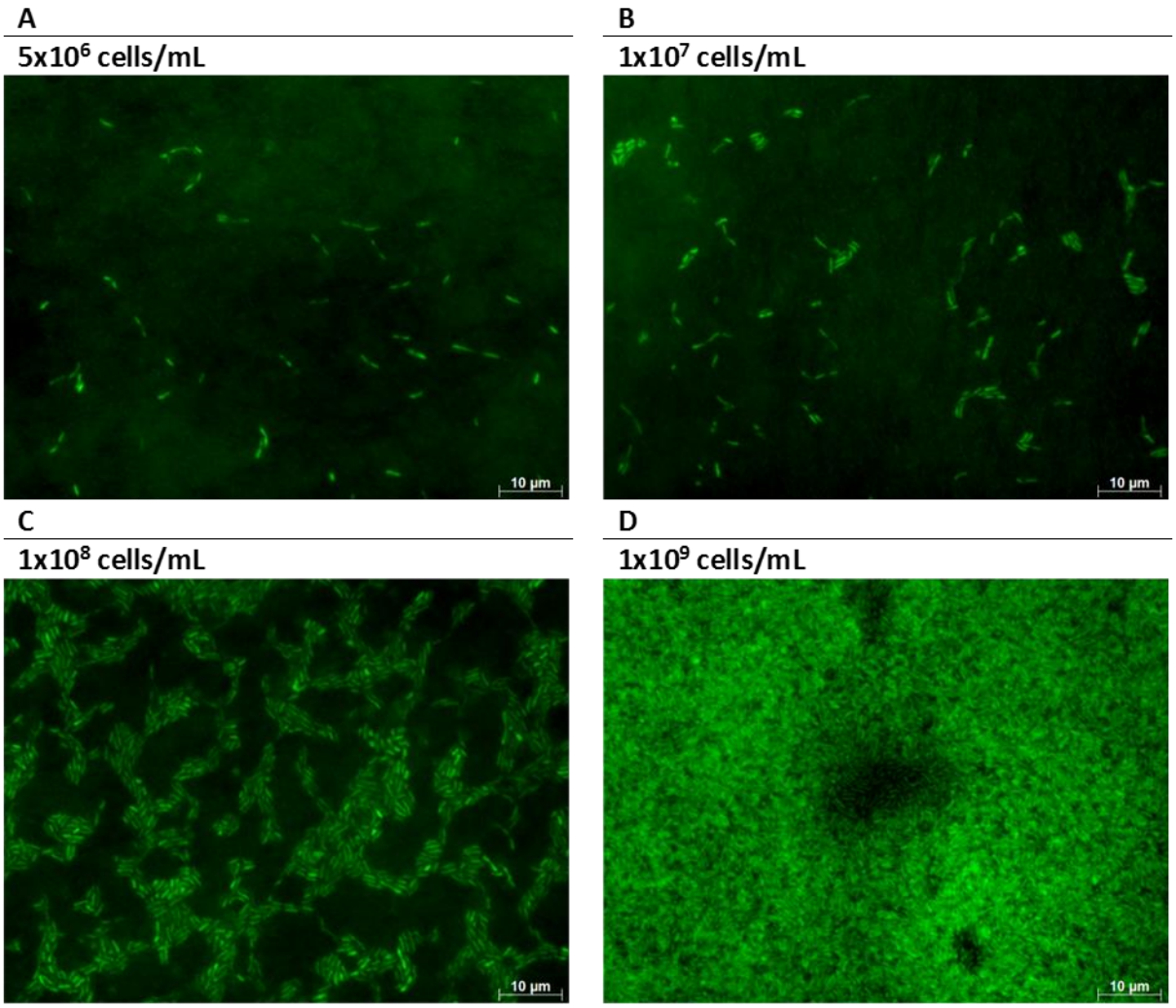

Figure 5: Distribution of *V. alginolyticus* cells on 0.2 µm GTTP filter. The cells (green) were stained with SYBR Green I. The desired distribution of cells separated inside the filtration area was achieved using 1 mL of a cell suspension containing $5x10^6$ cells/mL. The highest concentrations ($1x10^8$ or $1x10^9$ cell/mL) resulted in large cell groups up to a dens filter cake. (Scale bar 10 µm)

3.3.2. Fluorescent dyes for Raman spectroscopy

The prerequisite for a fast and selective identification of *Vibrio* is that single cells can be differentiated from the background. When using sample carriers, like filters, this can be achieved by staining the cells.

Carboxyfluorescein diacetate succinimidyl ester (CFDA SE):
It was not possible to achieve a satisfying staining of *V. alginolyticus* with CFDA SE, using the recommended protocol with an incubation time of 45 min. The fluorescent signal was very weak and faded too fast to take images. As positive control for the staining protocol, *E. coli* cells were stained. The staining of *E. coli* was successful (Figure 6). Longer incubation times or higher dye concentrations to improve the staining procedure were not tested.

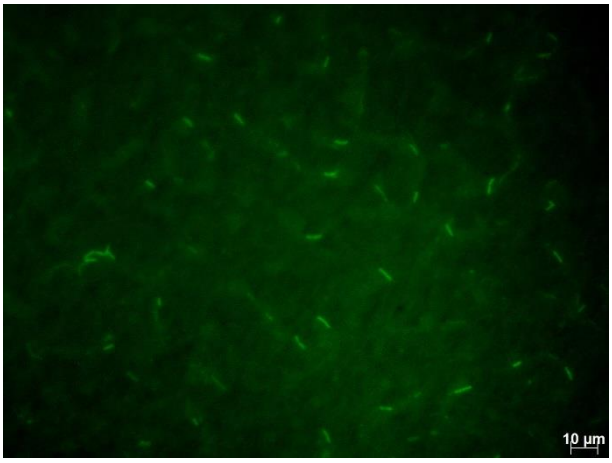

Figure 6: CFDA SE stained *E. coli* cells (green). It was possible to stain *E. coli* cells with this dye. The non-fluorescent CFDA SE diffused into the cells and was enzymatically converted to the fluorescent CFDA. (Scale bar 10 µm)

SYTO 9:

V. alginolyticus cells were successfully stained using the nucleic acid stain SYTO 9. The use of 0.12 µM SYTO 9 was sufficient to achieve a satisfying cell staining (Figure 7). Cells stained with SYTO 9 were also transferred to nickel slit filters, which will be described in section 3.4 (Figure 10).

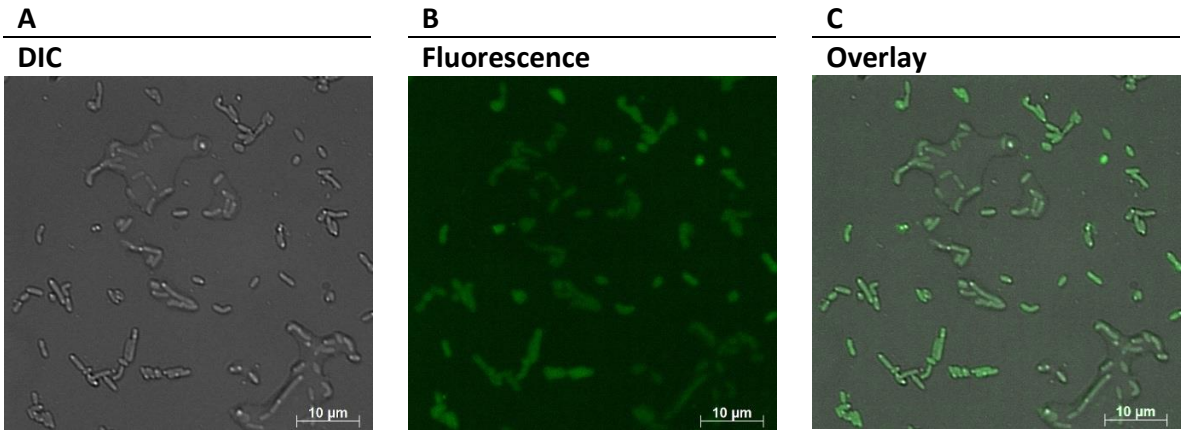

Figure 7: SYTO 9 stained *V. alginolyticus* cells (green) on glass slide. An overlay (C) of the DIC (differential interference contrast) image (A) and the fluorescence image (B) was produced to investigate if all cells were stained. (Scale bar 10 µm)

3.3.3. Metal array

It was not possible to load a filter with all samples completely transferred to the filter, as the fluids of some samples always remained inside the holes of the metal array. Another problem was that the resulting spots mixed with other spots close by or sometimes even more cells could be found around the actual spot position than inside it (Figure 8B). These spots seemed almost devoid of cells, but were surrounded by a dens carpet of cells. Differences could be seen when using the array in the two possible orientations (upright or upside down). Using the array in the upright orientation resulted in spots with blurred edges and cells spreading into the gap between the spots (Figure 8A). Using the array upside down worked better as more cells passed the holes, resulting in spots with sharp edges (Figure 8C). Although some spots were promising, others showed a completely different picture. As it was the case when using the array the right side up, more cells were observed surrounding the actual spot than within (Figure 8D).

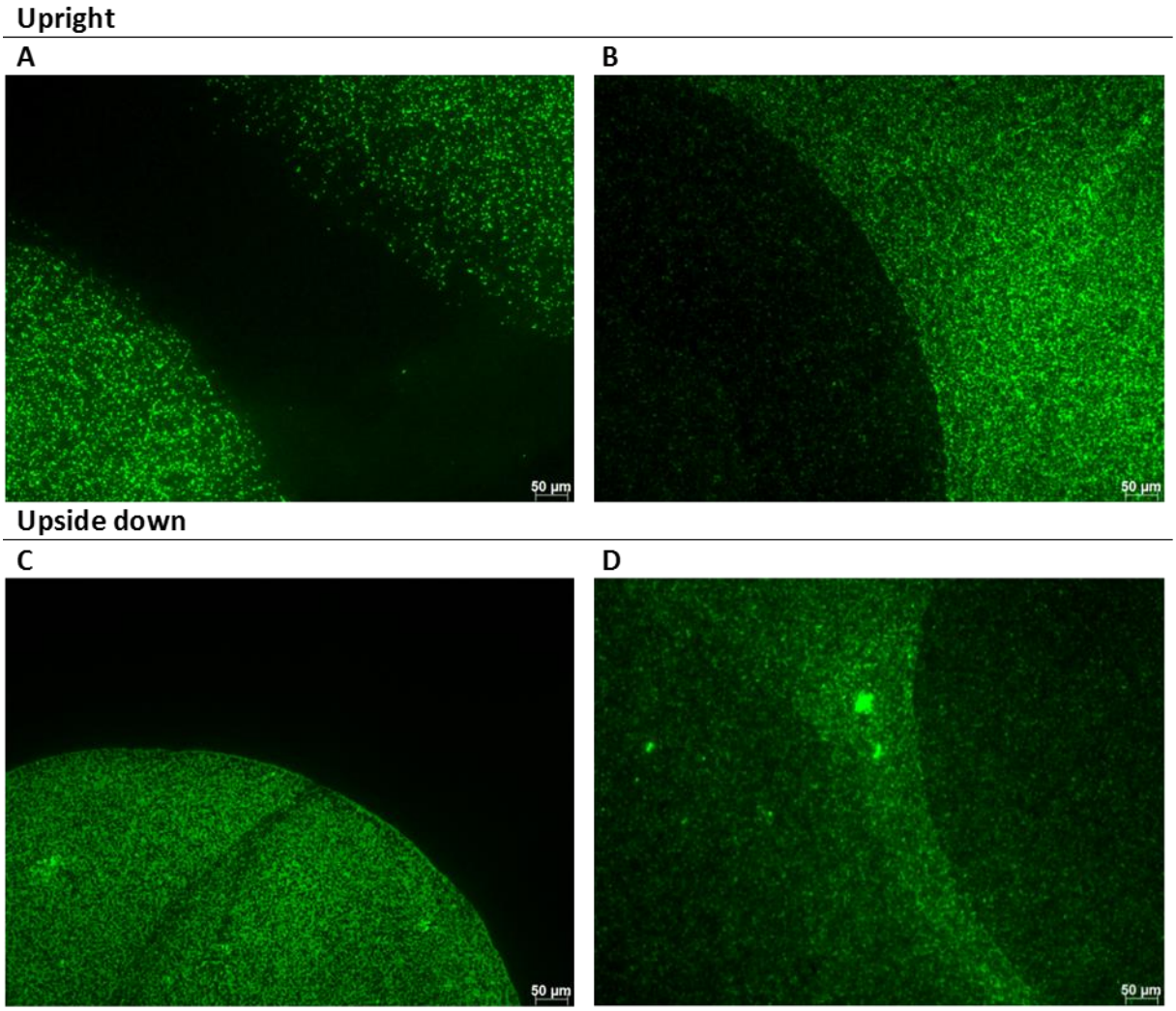

Figure 8: Fluorescence microscopy of spots generated using the metal array. *V. alginolyticus* cells were stained with SYBR Green I (green). Spots with blurred edges were generated when using the array in the upright orientation (A). Using it upside down created spots with sharp edges (C). In both orientations, positions with more cells surrounding the spot area where detected (C & D). (Scale bar 50 µm)

Gradually changing the applied vacuum during as well as between filtrations from 200 mbar up to 600 mbar did not improve the transfer of the samples. The best result was achieved with an applied vacuum of 400 mbar, an 8 µm cellulose nitrate backing filter below the 0.2 µm GTTP filter and while using the metal array upside down. But still not all samples were transferred to the filter. The metal array was not used for further filtrations.

3.4. Nickel slit filters and silver membrane filters

The nickel slit filters had elongated pores with a width of approx. 0.3 - 0.4 µm at the narrowest point. The upper part of the pore is "tub" shaped and was measured in the BPE to be 30 µm x 3.6 µm (Figure 9A). In bright field mode, the whole surface of the filter and reflections from inside the "tubs" were detected as particles (Figure 9A binarized image). In dark field mode, the edges of the slits reflected the incident light and interfered with the particle recognition (Figure 9B, binarized image). As no structurally conditioned artefacts were found in fluorescence mode, SYTO 9 stained *V. alginolyticus* cells ($1x10^8$ cells) were filtered onto a nickel slit filter.

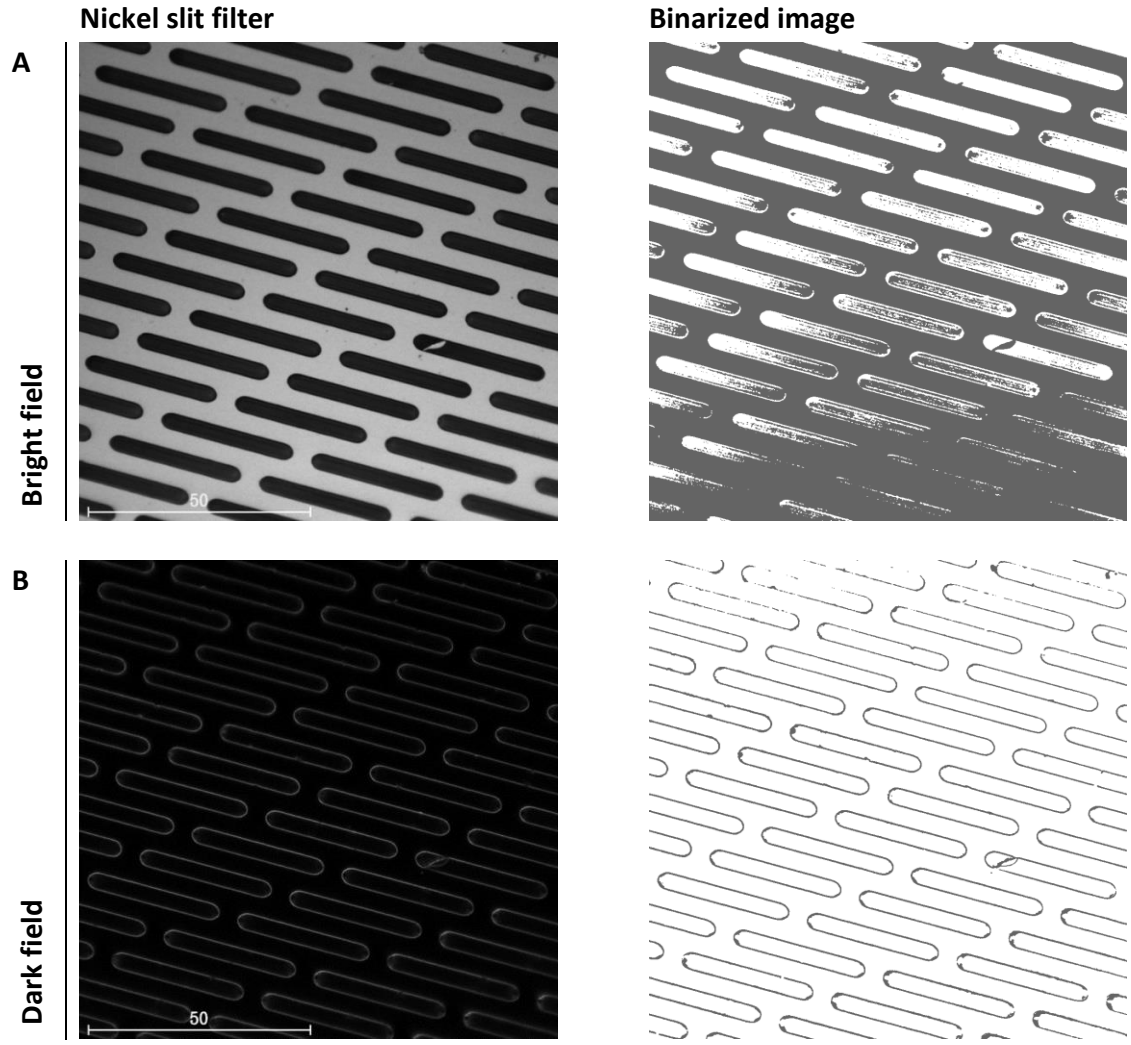

Figure 9: Microscopy of nickel slit filters. The size of the filter pores (30 µm x 3.6 µm) was measured in bright field mode (A). In the binarized image the whole surface of the filter was detected as particle, as well as some reflections from inside of the pores. The planar nickel filter surface as well as the pore "tubs" appeared black, but the edges of the slits reflected the light and were therefore detected as particles (B). This interference made the nickel slit filters unsuited for the use in dark field mode. (Scale bar 50 µm)

Additional to the cells, drops of various sizes could be seen in bright field mode (Figure 10A) but were not detected in fluorescence mode (Figure 10B). The fluorescence of the cells remained but the number of observed cells was lower than expected. Fluorescence signals were seldom found on the planar surface of the filters, but mostly inside the “tubs” (Figure 10C).

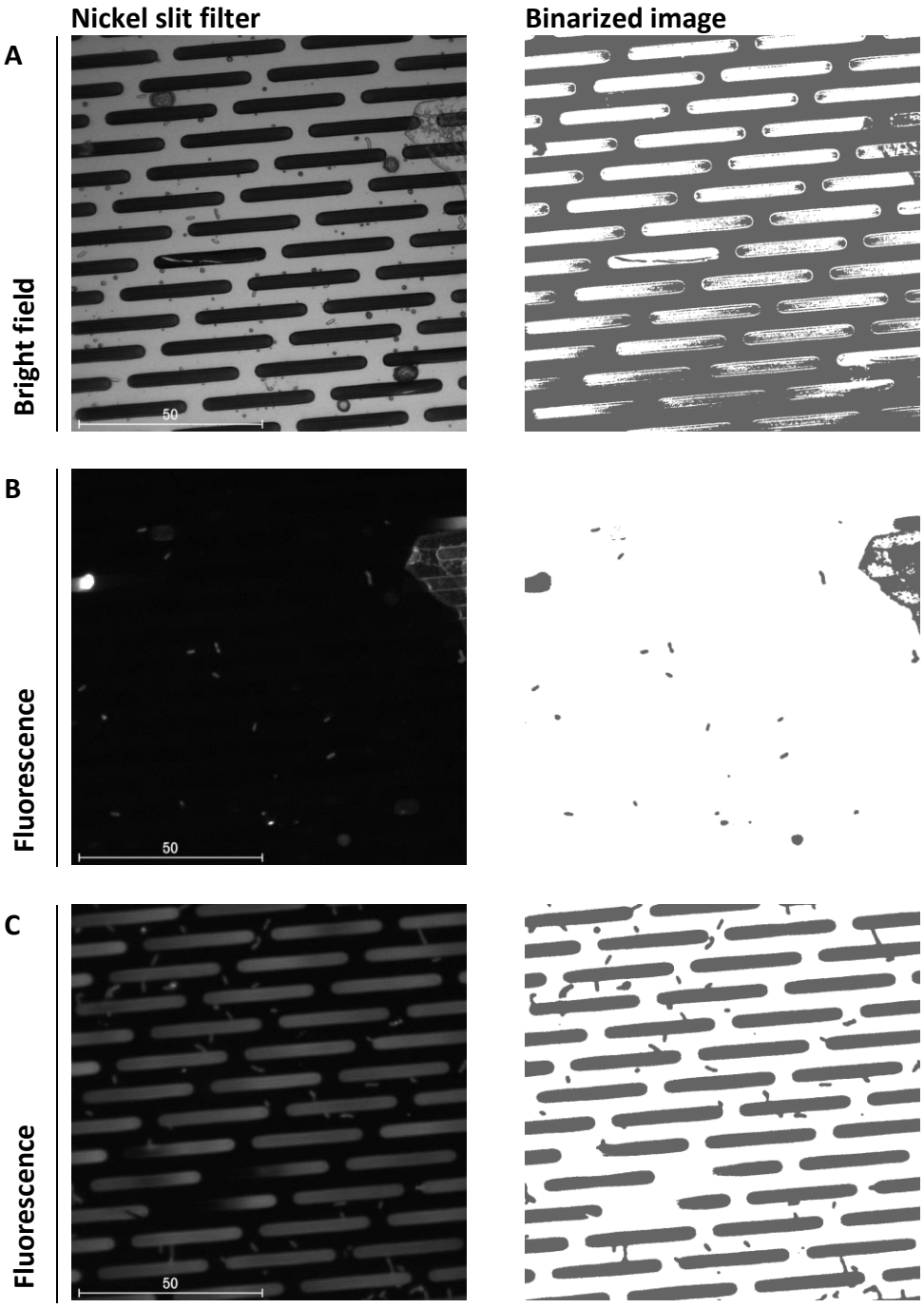

Figure 10: Fluorescence microscopy of *V. alginolyticus* on nickel slit filters. Not only cells but smaller and larger, drop shaped particles could be seen (A). In fluorescence mode, most of these particles gave no signal at all or faded fast, while the cells maintained their fluorescence (B). The lowest row of images was taken at another position of the same filter (C). Strong fluorescence signals were visible inside the pores but those signals faded within a few seconds. (Scale bar 50 µm)

Raman measurements were performed inside the pores (Figure 11) and spectra of bacterial cells could be detected. It can be assumed that cells filtered onto the nickel slit filters ended up inside the “tub” of the slits. It was not possible to see how many cells were pulled into these pore openings. This made a quantitative statement impossible and the nickel slit filters were no longer used for further experiments.

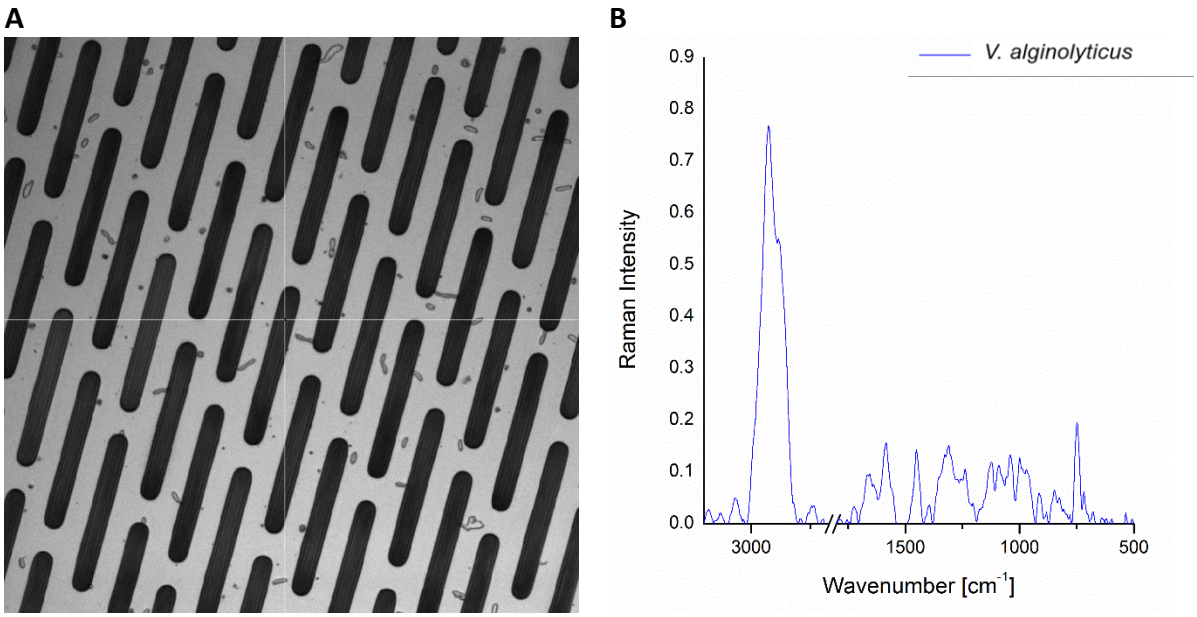

Figure 11: Raman measurement performed inside a “tub” of a nickel slit filter. The position was automatically marked by the BPE through the white lines (A). The corresponding spectrum is shown on the right side (B).

As an alternative to nickel slit filters, silver membrane filters were tested, because silver is also Raman inactive. The silver membrane filters have an absolute pore size of 0.2 µm and are generated from granular silver particles. The granular structure results in a rough filter surface with cavities and plateaus (Figure 12A). The irregular cavities between the plateaus had sizes larger than 1.5 µm. Similar to the nickel slit filters, the three-dimensional structure of the silver membrane filter interfered with the particle recognition in dark field mode (Figure 12B). Even filters without cells showed fluorescence signals (Figure 12C). After filtration of cells onto the filter, the distinction of fluorescing cells and background fluorescence was not possible.

The handling of both metal filter types was extremely challenging. The filtration setup was almost impossible to seal without affecting the integrity of the filters. The edges were easily bent during filtration, which resulted in problems in focussing the sample plane in the BPE.

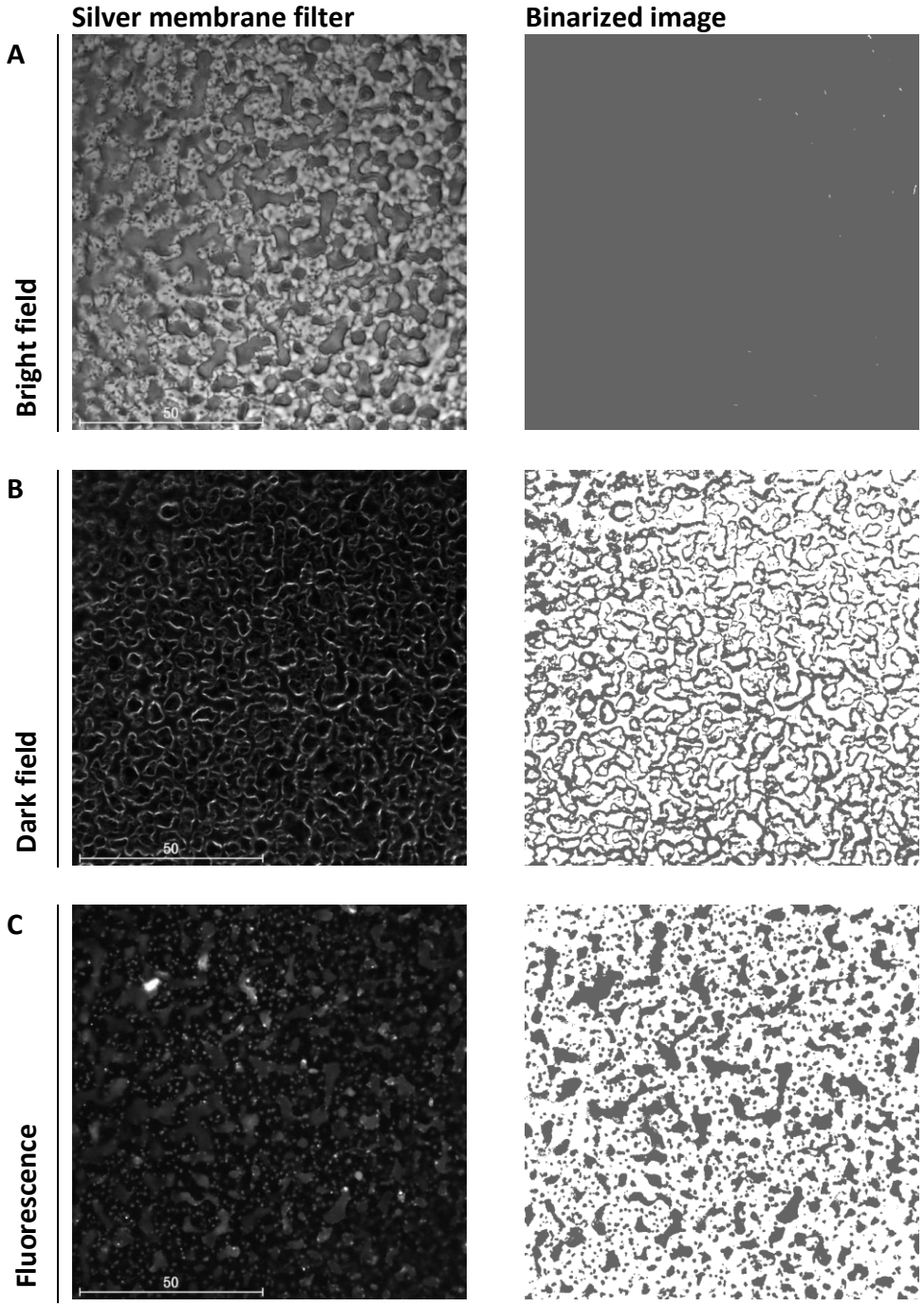

Figure 12: Microscopy of empty silver membrane filter. In bright field mode, the rough surface of the filter appears as plateaus and cavities (A). The edges of this granular structure made a correct particle recognition via dark field mode impossible (B). Fluorescence signals of the filter material were detected without cells (C). (Scale bar 50 µm)

3.5. Nickel foil

Since the samples had to be applied to the nickel foil by spotting, the result from "Cell concentration determination" (3.3.1) could not be transferred directly. In order to detect well-distributed cells, different drop volumes and concentrations were tested. Regardless of the drop volume, suspensions with $1x10^9$ or $1x10^8$ cells/mL were concentrated too high or too low respectively, so a concentration between these values two was chosen ($5x10^8$ cells/mL). At constant concentration of the cell suspension, the distribution of cells worsened with increasing drop volume. Drops of 10 µL or 20 µL were unsuitable as the cells were too widely dispersed. Compared to 3 µL drops, 5 µL drops were easier to handle, as the removal of the drop could be performed in a more fluid movement, which resulted in a better distribution of the cells. The best results were achieved with cell suspensions containing $5x10^8$ cells/mL and a drop volume of 5 µL (Figure 13A).

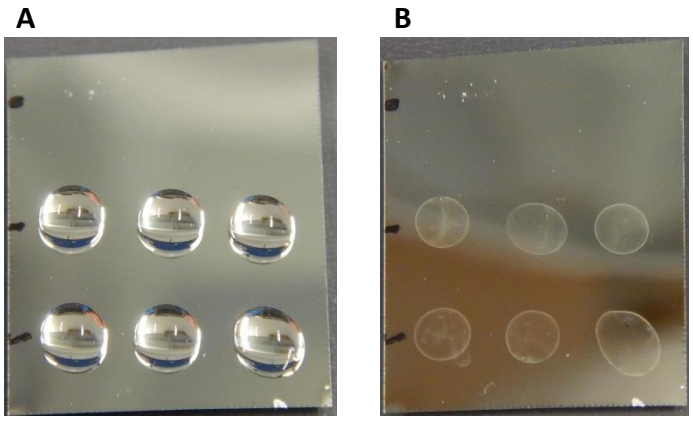

Figure 13: Bacterial suspension and acetaminophen (APAP, small white particles in the top row) on nickel foil. Drops of 5 µL were spotted (A) and taken off again after 5 min. The dried samples were still visible (B). The positions of the rows were marked with a waterproof marker (black spots) to simplify the examination under the microscope.

It was not possible to remove the suspension completely, but the remaining liquid dried up within a few s. In every case, high numbers of cells accumulated at the edges of the spots (Figure 13B). The remaining liquid either covered the whole spot area or formed smaller drops within the spot. These smaller drops contained more cells than the surrounding areas and, again, higher numbers of cells accumulated at the edges (Figure 14A). In Figure 14B a sample of *V. alginolyticus* cells is shown, where salt crystals formed as dendritic structures. It is unclear which substances crystallized, but they presumably were media components, which had been insufficiently removed before applying the sample to the foil. The cells within the sample gathered at the ends of the dendritic structures and lost their native structural appearance. On this sample, no Raman measurement was performed, as it was assumed that the integrity of the spectra was lost.

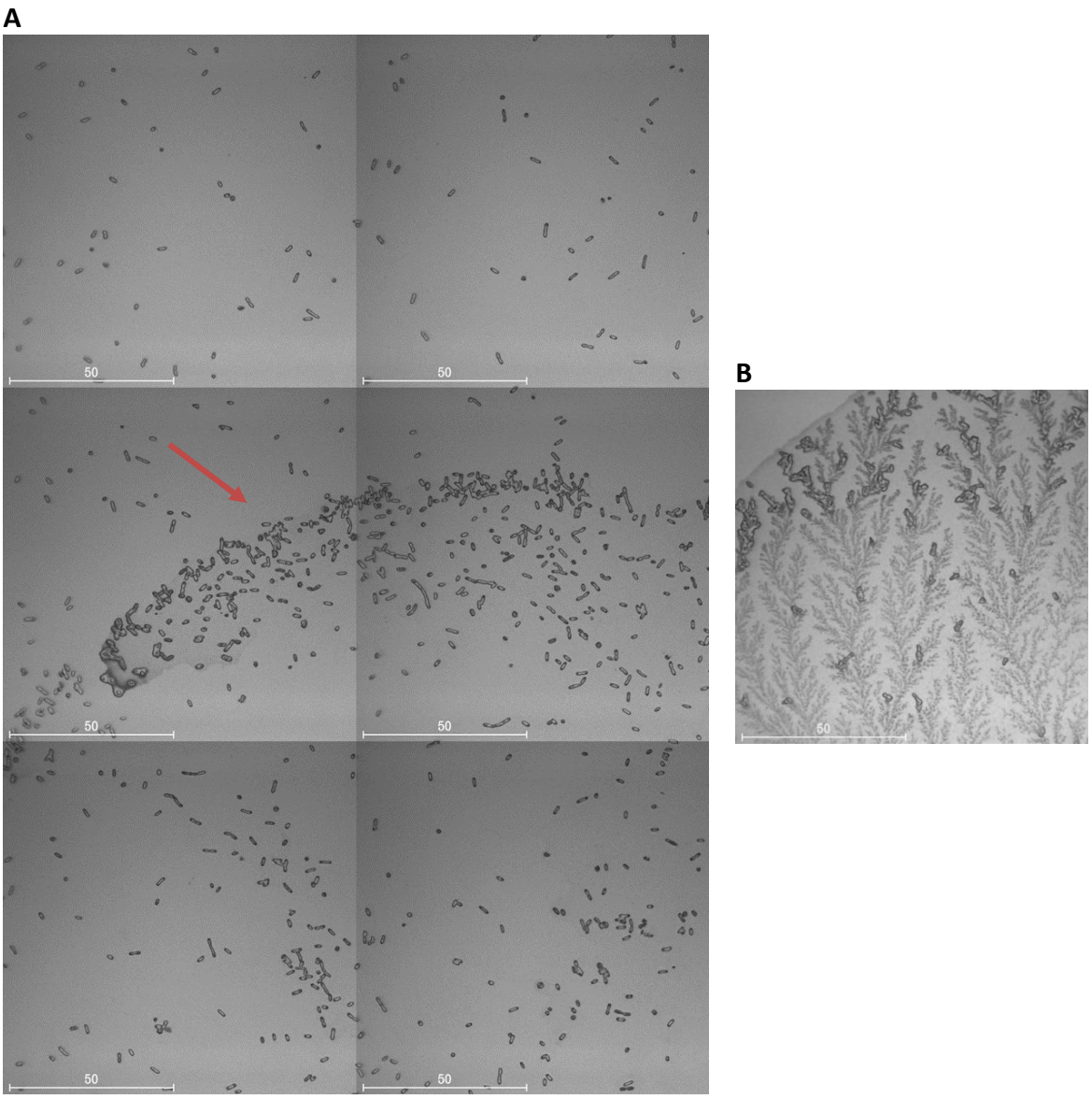

Figure 14: Distribution of *V. alginolyticus* cells on nickel foil (A). More cells were found inside the drying spot and were closer together than the cells surrounding it. The edge of the inner spot appears as curved line along which many cells clustered (marked with red arrow). Drop volume was 5 µL, cell concentration of used suspension was $5x10^8$ cell/mL.
Salt in sample (B). Drying spot with dendritic structures which might originate from salts that were not removed from the cell suspension. (Scale bar 50 µm)

3.6. Particle recognition and automatic selection

3.6.1. Threshold

To ensure correct particle recognition and selection during the automatic measurement, a binarization threshold suitable for the sample is required. Greyscale values between 200 and 240 were tested (Figure 15). Setting the threshold below 210, the cell detection was incomplete and some cells looked thinner than they were or were detected as dumbbell-shaped particles. With values higher than 230, too many pixels were detected and assigned to the cells. Adjacent cells were merged and could not be recognized separately. The value of 225 was chosen, because most cells were recognised correctly and a separation of neighbouring cells was still possible, provided that they were not attached to each other.

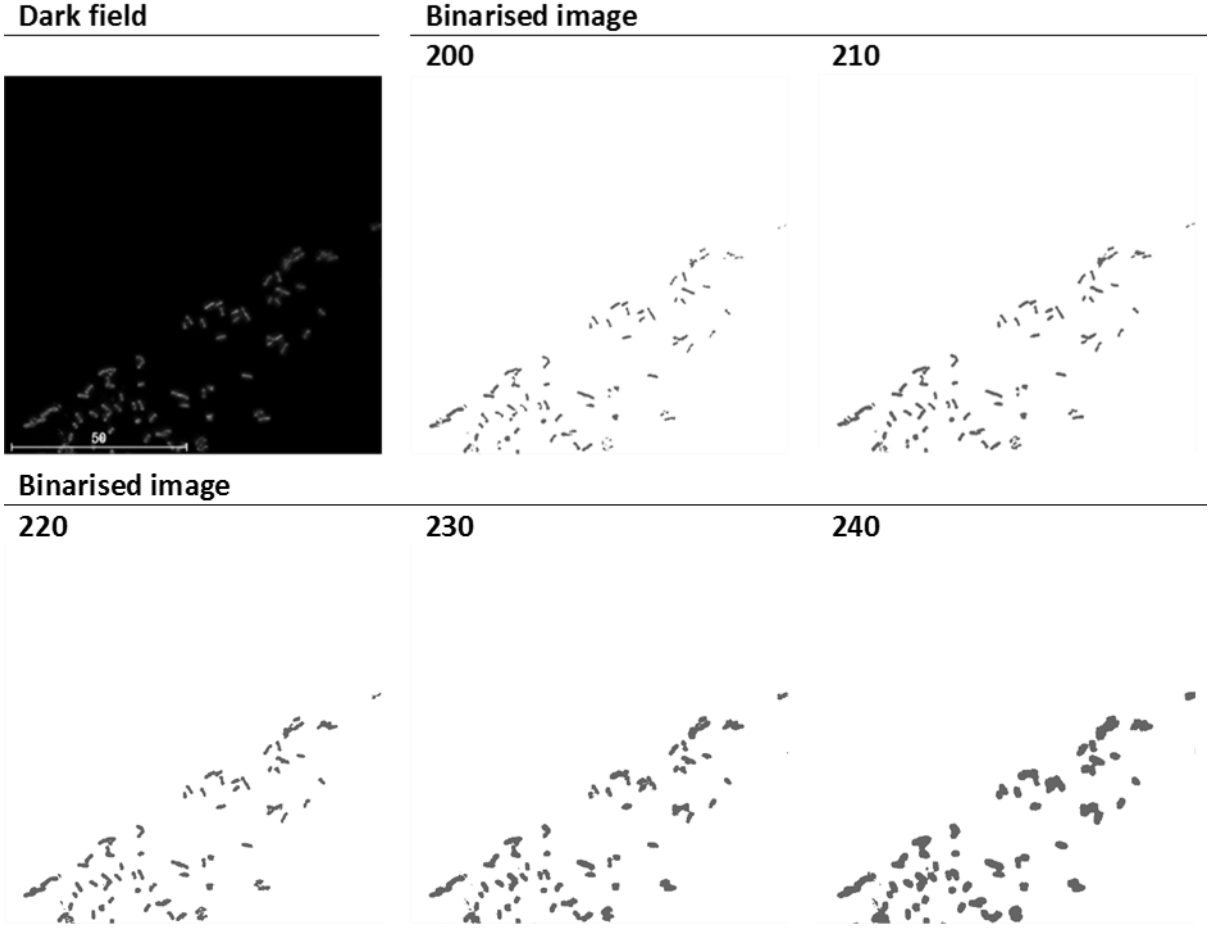

Figure 15: Images binarized using different threshold values. The values 200 and 210 led to an incomplete cell detection. Above 230, too many pixels were assigned to the cells and adjacent cells were merged to single particles. (Scale bar 50 µm)

3.6.2. Size and Elongation

The strains varied in size and, therefore, specific size and elongation ranges were chosen for the automatic analyses (Figure 16). For *V. alginolyticus* and *V. parahaemolyticus*, which were larger than the other three strains, particles within a size range form 2.0 - 4.0 µm and with an elongation range between 1.4 - 2.5 µm were selected for analysis. For *V. cholerae*, *V. mimicus* and *V. vulnificus* the size range was set from 1.0 - 3.0 µm, with an elongation range between 1.3 - 2.0 µm.

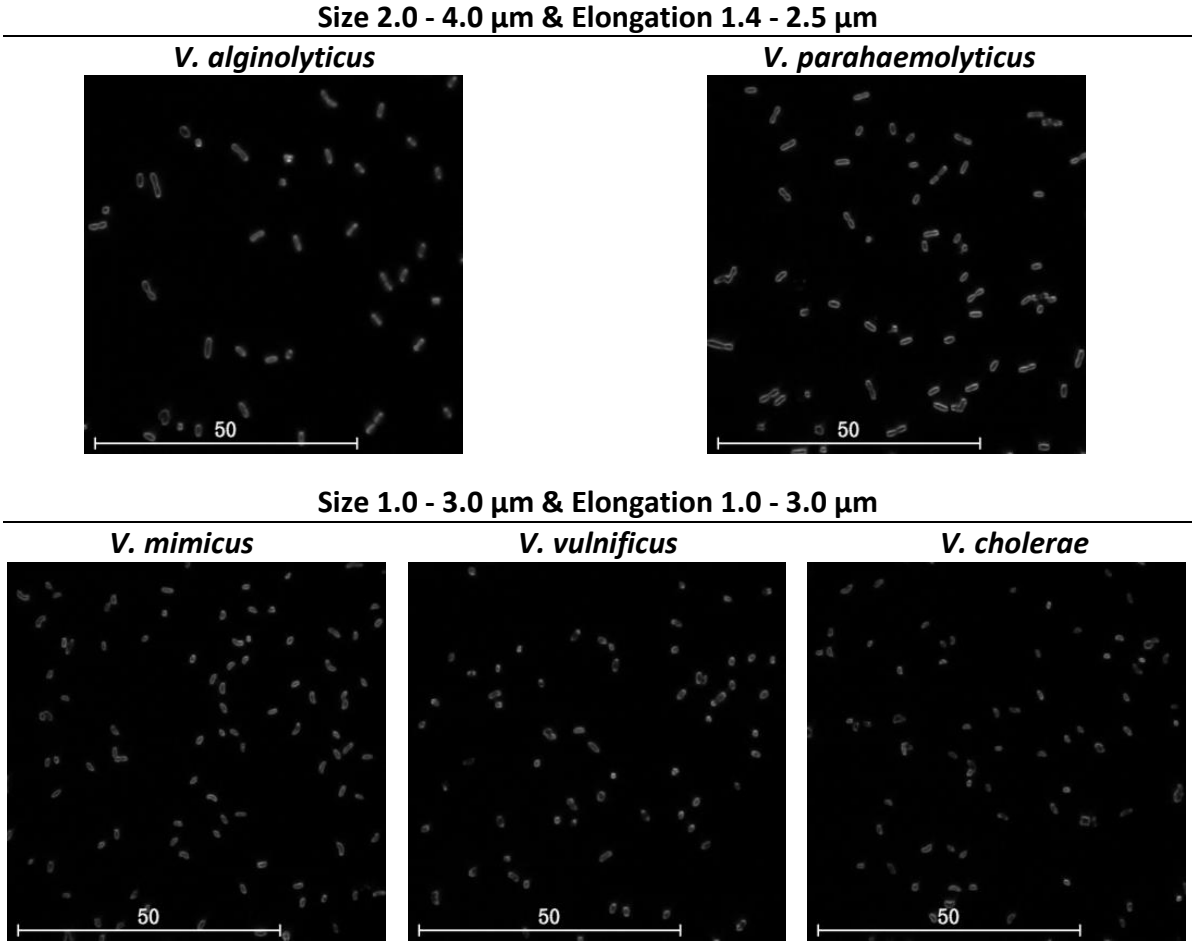

Figure 16: Dark field microscopy of *Vibrio* spp. *V. alginolyticus* and *V. parahaemolyticus* cells were larger than *V. mimicus*, *V. vulnificus and V. cholerae* cells. For the automatic measurements, two defined size and elongation ranges were chosen, respectively. (Scale bar 50 µm)

3.7. Laser intensity

The experiment was started using a laser intensity of 7.5 mW, which led to satisfying spectra for *V. alginolyticus* and *V. parahaemolyticus* cells but not for the other three species. The laser intensity was then adapted to 15.75 mW for *V. cholerae*, *V. mimicus* and *V. vulnificus*. This led to an increase in the overall Raman intensity of the spectrum. To show the difference between the two used laser intensities, exemplary spectra of *V. cholerae* were plotted in Figure 17, showing the raw spectra in the upper part and the corresponding pre-processed spectra (by ACCU) in the lower part.

The increased laser intensity led to an elevation of the baseline signal and enhanced bands in the CH-stretch (2800 cm^{-1} - 3050 cm^{-1}) as well as in the fingerprint region (585 cm^{-1} - 1750 cm^{-1}). The noise-to-signal ratio was improved from approximate values below 20 to values higher than 30. After the pre-processing, the bands in both spectra were raised to comparable Raman intensities but in the spectrum obtained with 7.5 mW signals, which do not correspond to the biological sample, were raised from the noise signal as well. The band intensities were highly different in the two spectra.

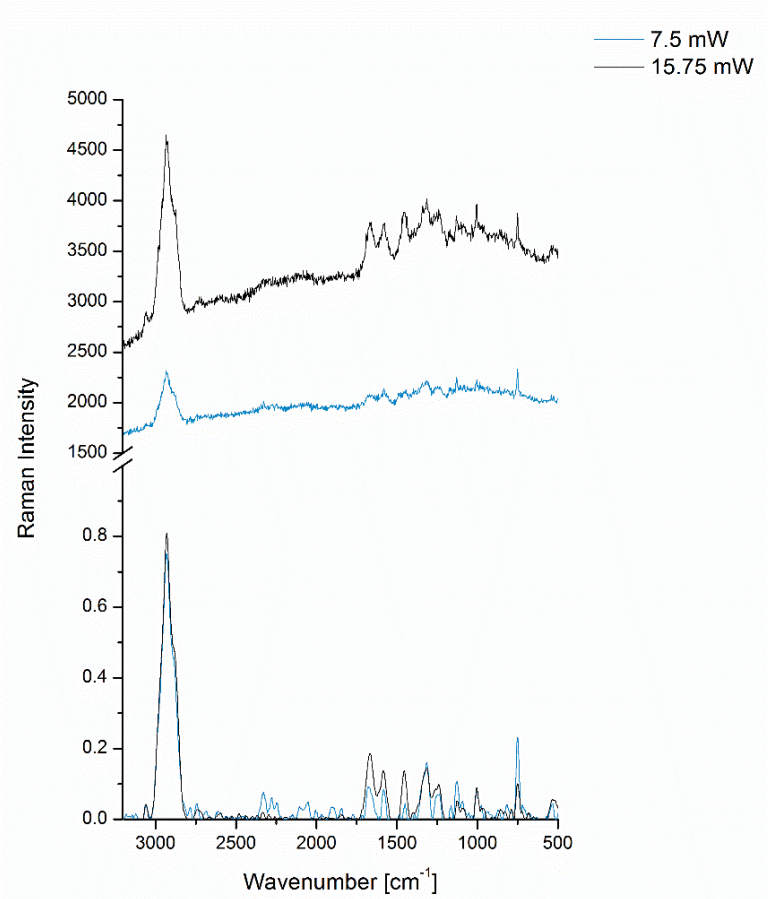

Figure 17: Differences in Raman spectra due to changed laser intensity. Raman spectrum of *V. cholerae* obtained with 7.5 mW (blue) and 15.75 mW (black). The upper part shows the raw spectra the lower part "BPE pre-processed" spectra.

3.8. Identification of different *Vibrio* spp. via Raman spectroscopy

3.8.1. Spectra

Raman spectra contain information about different molecular vibrations and, therefore, about the chemical composition of the analysed bacteria. The knowledge about vibrational modes allows the assignment of Raman bands to specific functional groups, bonds or molecules (Figure 18A). By looking at these possible assignments, four prominent bands were detected at 749, 1129, 1310 and 1584 cm^{-1}. These bands were present within the spectra of all five analysed *Vibrio* spp. and could be assigned to the protein cytochrome c by comparison to the spectrum of the pure substance (Figure 18B). The spectrum of pure cytochrome c was provided by Dr. Anja Silge.

A

Wavenumber [cm^{-1}]	Assignment
585 - 1750	Fingerprint region
720	adenine
722	$\rho(CH_2)$
749	thymine ring, **cytochrome c**
785	cytosine, uracil
810	C-O-P-O-C in RNA backbone
828	exposed tyrosine
855	buried tyrosine
955	$\rho(CH_3)$ terminal
1003	phenylanlanine
1032	*v*(CC) skeletal, cis
1200 - 1280	amide III
1129	**cytochrome c**
1173	*v*(C-N), *sec* amine, aliphatic
1310	**cytochrome c**
1335	*v*(C-N), amine, aromatic
1340	DNA (A, G)
1575	amide II
1584	**cytochrome c**
1650 - 1680	amide I
2800 - 3050	CH-stretch region
3129	*v*(CH) olefinic

v - stretching, *ρ* - rocking

B

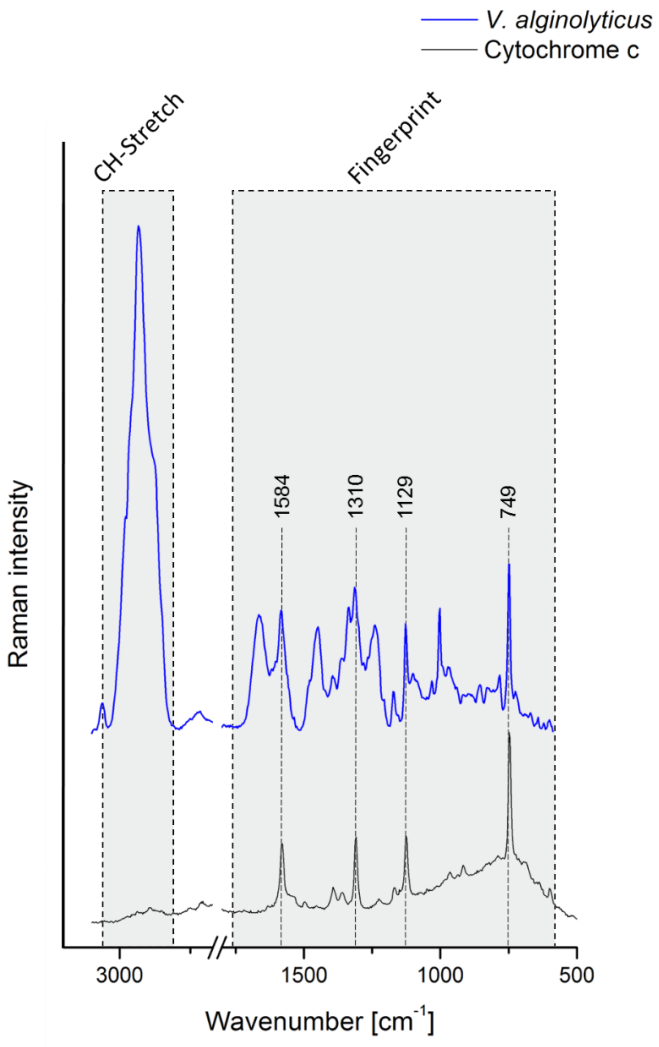

Figure 18: Assignment of some bands found in *Vibrio* spp. spectra (A). The spectra can be sectored into the CH-stretch and the fingerprint region (highlighted in grey). The mean spectrum of *V. alginolyticus* (blue) was compared to the spectrum of cytochrome c (black) (B). For better display the spectra were shifted along the y-axis. Band assignment according to (Williams and Edwards, 1994; Maquelin et al., 2002; Harz et al., 2005; Chan et al., 2007; Lambert et al., 2012)

The mean spectra of all five *Vibrio* spp. showed high resemblance to each other (Figure 19). Thus, it was not possible to distinguish the species solely via investigation by eye. Comparing the mean spectra of both data sets, “BPE” and “Jena” showed different effects of the pre-processing. The dimensions of the Raman intensity range between 0 to 0.8 (BPE) and 0 to 0.2 (Jena) arbitrary units. In this study, differences can be neglected, as the comparison of spectra and their respective intensities were considered only within the separated data sets. The standard deviation (grey shades) was higher for some bands in the Jena data set. The spectral resolution seemed reduced in the BPE data set. One of the results was a change in the spectral range from 1290 to 1340 cm^{-1} (grey dashed box, Figure 19). While the “Jena” spectra showed two separate band peaks in this region, the bands in the BPE spectra were fused to one peak. In this range, cytochrome c (1310 cm^{-1}) and stretching mode C-N bonds within aromatic amines can be detected.

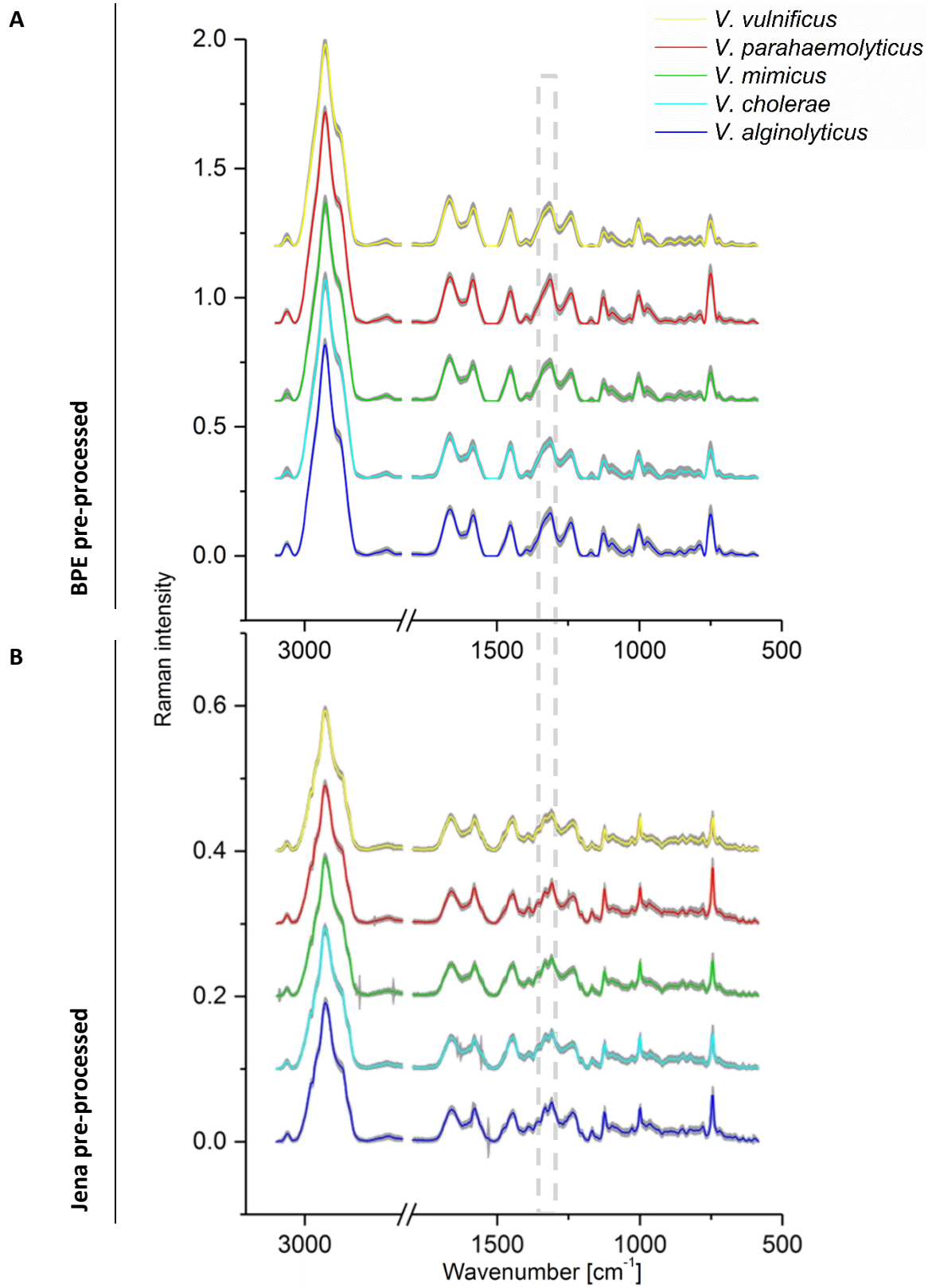

Figure 19: Mean Raman spectra and standard deviation (grey shades) of *Vibrio* spp. In both data sets the spectra show a high resemblance and consist of the same Raman bands with different intensities. The spectral resolution was reduced during the BPE pre-processing. The resulting effect could be seen in the spectral range from 1290 to 1340 cm^{-1} (grey dashed box).

3.8.2. Statistical analysis

Multivariate analysis

The one-way PERMANOVA main test provided the information, that there was a difference between the *Vibrio* spp. in both pre-processed data sets (Table 6). The permutation results, with low p-values (BPE & Jena = 0.001) and high pseudo-F values (BPE = 35.387; Jena = 22.882), indicate strong evidence against the null hypothesis, which claims, that there are no more differences between the species except the usual variations. As revealed by the two-way PERMANOVA main tests, the variance between *Vibrio* species could be explained by the factor "species" whereas the factor "batch" which corresponds to the different measurement days, had no significant influence (Table 7)

Table 6. Results of the one-way PERMANOVA main-test. The test showed that there was a difference in variances between the analysed *Vibrio* spp. in both data sets. (Significance level defined as p(perm) > 0.05)

"BPE"					
Source	df	SS	MS	Pseudo-F	p(perm)
Species	4	9237.3	2309.3	35.387	0.001
Residual	1250	81574	65.259		
Total	1254	90811			

"Jena"					
Source	df	SS	MS	Pseudo-F	p(perm)
Species	4	4094.6	1023.7	22.882	0.001
Residual	1250	55921	44.737		
Total	1254	60015			

df = degrees of freedom, SS = sum of squares, MS = mean square

Table 7. Results of the two-way PERMANOVA main-test. The different measurement days (factor "batches") had no significant influence on the separation of the data groups ("species"). (Significance level defined as p(perm) > 0.05)

"BPE"					
Source	df	SS	MS	Pseudo-F	p(perm)
Species	4	9055.4	2263.8	8.3807	0.001
Batch	2	602.9	301.45	1.1142	**0.363**
Species vs. Batch	8	2173.7	271.71	4.2768	0.001
Residual	1240	78779	63.532		
Total	1254	90811			

"Jena"					
Source	df	SS	MS	Pseudo-F	p(perm)
Species	4	3949.3	987.33	4.6319	0.002
Batch	2	475.18	237.59	1.1127	**0.344**
Species vs. Batch	8	1715.7	214.47	4.9487	0.001
Residual	1240	53739	43.338		
Total	1254	60015			

df = Degrees of freedom, SS = sum of squares, MS = mean square

The pair-wise comparison of the species was performed on the whole spectra, as well as on the fingerprint region and the CH-stretch region separately. The different pre-processing methods delivered similar results, with a few exceptions, which are summarized in the next section.

"BPE pre-processing":
The whole spectra, as well as the fingerprint region alone, were sufficient to explain the variance between all species. The species comparisons resulted in highly significant p- and t-values (Table 8). In 9 of the 10 possible comparisons, significant differences could be found in the CH-stretch region. Only the species *V. cholerae* and *V. mimicus* differed insignificantly in the CH-stretch (p(perm) = 0.168, t = 1.1878).

Table 8. One-way PERMANOVA pair-wise test of the "BPE pre-processed" data set. The comparisons of the whole spectrum, as well as the comparisons of the fingerprint regions, led to significant differentiation of the species. The CH-stretch region was sufficient for all but one of the compared groups. The variances of *V. cholerae* and *V. mimicus* could not be separated in the CH-stretch region (highlighted in bold). Significance level was defined as p(perm) > 0.05

"BPE"	Whole spectrum		Fingerprint		CH-stretch	
Comparison	t	p(perm)	t	p(perm)	t	p(perm)
V.a.* vs. *V.c.	7.2167	0.001	6.4908	0.001	9.6695	0.001
V.a.* vs. *V.m.	6.3498	0.001	5.4829	0.001	9.1946	0.001
V.a.* vs. *V.p.	2.9241	0.001	3.114	0.001	1.8918	0.002
V.a.* vs. *V.v.	6.505	0.001	6.6295	0.001	6.1302	0.001
V.c.* vs. *V.m.	2.7847	0.001	3.0309	0.001	**1.1878**	**0.168**
V.c.* vs. *V.p.	7.6227	0.001	7.0739	0.001	9.5918	0.001
V.c.* vs. *V.v.	4.8263	0.001	4.8271	0.001	4.6665	0.001
V.m.* vs. *V.p.	7.2072	0.001	6.7285	0.001	9.0126	0.001
V.m.* vs. *V.v.	3.4548	0.001	3.1637	0.001	4.3742	0.001
V.p.* vs. *V.v.	7.5502	0.001	7.8098	0.001	6.421	0.001

V.a. = V. alginolyticus, *V.c. = V. cholerae*, *V.m. = V. mimicus*, *V.p. = V. parahaemolyticus*, *V.v. = V. vulnificus*

"Jena pre-processing":

Differences between the species could be found comparing the whole spectra, the fingerprint region as well as the CH-stretch region. In contrast to the "BPE pre –processing" data set, this was also true for the CH-stretch region comparison of *V. cholerae* and *V. mimicus*. It should be noted, that, although the difference between the two species was highly significant, the small t-value indicated that the evidence against the null hypothesis was not as strong as it was in the other comparisons and regions.

Table 9. One-way PERMANOVA pair-wise test of the "Jena pre-processing" data set. All compared groups showed a high significance in the variances. The smallest t-value of all comparisons (CH-stretch, *V. cholerae* vs. *V. mimicus*) was highlighted in bold. (Significance level defined as p(perm) > 0.05)

"Jena"	Whole spectrum		Fingerprint		CH-stretch	
Comparison	t	p(perm)	t	p(perm)	t	p(perm)
V.a.* vs. *V.c.	5.1502	0.001	5.2579	0.001	4.5088	0.001
V.a.* vs. *V.m.	4.1022	0.001	4.2261	0.001	3.6102	0.001
V.a.* vs. *V.p.	3.0673	0.001	3.2402	0.001	2.4706	0.001
V.a.* vs. *V.v.	4.6683	0.001	5.0709	0.001	2.9246	0.001
V.c.* vs. *V.m.	2.6383	0.001	2.7978	0.001	**1.9223**	0.001
V.c.* vs. *V.p.	6.6997	0.001	7.0629	0.001	5.1367	0.001
V.c.* vs. *V.v.	3.8352	0.001	3.8894	0.001	3.5857	0.001
V.m.* vs. *V.p.	6.0874	0.001	6.508	0.001	4.5248	0.001
V.m.* vs. *V.v.	3.0516	0.001	2.9644	0.001	3.3272	0.001
V.p.* vs. *V.v.	6.426	0.001	7.2048	0.001	2.7725	0.001

V.a. = V. alginolyticus, *V.c. = V. cholerae*, *V.m. = V. mimicus*, *V.p. = V. parahaemolyticus*, *V.v. = V. vulnificus*

In order to analyse the distribution of the data, the "BPE" data set was chosen as example. The group centroids were calculated and a cluster analysis was performed for the whole spectra, the fingerprint region and the CH-stretch (Figure 20). The distance between the group centroids equals the distance between the species in the data set. The longer the distance, the more differences between the groups were found. Regardless of the underlying spectral region used, the *Vibrio* spp. clustered in a repeated pattern (Figure 20). *V. alginolyticus* and *V. parahaemolyticus* formed a group apart from the remaining three species, while *V. vulnificus* was clustered together with *V. cholerae* and *V. mimicus*. *V. cholerae* and *V. mimicus* seemed to have the same distance to each other as *V. alginolyticus* and *V. parahaemolyticus*. By taking a closer look at the different dendrograms it became apparent that the distances between the species changed, when the spectral region were considered separately. The heterogeneity within the fingerprint region was larger than in the CH-stretch region.

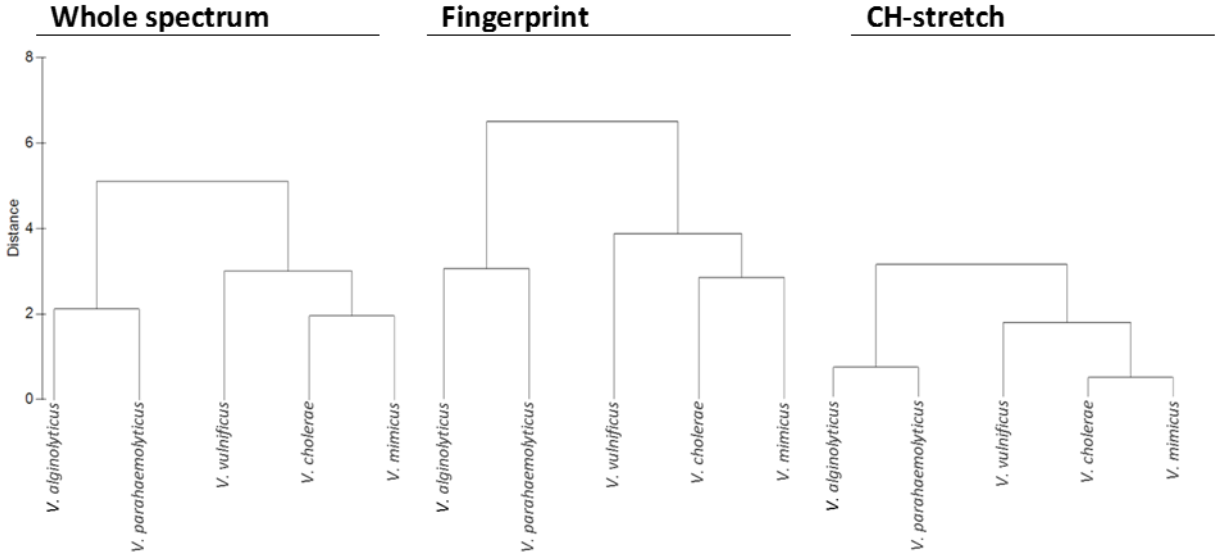

Figure 20: Cluster analysis of group centroids. The largest distance between the group centroids were obtained in comparison of the fingerprint region. The CH-stretch region had the lowest distances.

Similarity percentage (SIMPER) analysis showed that the dissimilarities of the species was different between the BPE and the Jena pre-processed data sets (Table 10). While the dissimilarities in the BPE set range from 11.29 % (*V. cholerae* vs. *V. parahaemolyticus*) to 12.63 % (*V. mimicus* vs. *V. vulnificus*), they were a few percent lower in the Jena set, where they range between 9.33 % (*V. cholerae* vs. *V. mimicus*) and 10.14 % (*V. parahaemolyticus* vs. *V. vulnificus*). Although single wavenumbers contribute little to the dissimilarities (< 0.45 %), in both data sets certain wavenumbers appear repeatedly with the highest contributions. Bands around 750, 840, 1138 and 1381 cm^{-1} had the biggest contribution in the "BPE" data set. The wavenumber values found did not exactly match these values but correspond to these bands. In the "Jena" data set, the two dominating wavenumbers (747 and 1536 cm^{-1}) were accompanied by two values that were not repeated at all.

Summarizing the wavenumber contributions within the different spectral regions showed that the fingerprint region explained 78.9 % (BPE) and 76.2 % (Jena) of the dissimilarities between the species while the CH-stretch explained only 20.8 % (BPE) and 23.2 % (Jena).

Table 10: Results of the SIMPER analysis for wavenumber contribution. The average dissimilarities between the species differ between the two data sets. The contribution of single wavenumbers was small but the highest contributing values appeared repeatedly in both data sets.

	Avg. dissimilarity		**Most contributing wavenumbers**			
	BPE	**Jena**	**BPE**		**Jena**	
Comparison	**[%]**		**[cm^{-1}]**	**[%]**	**[cm^{-1}]**	**[%]**
V.a.* vs. *V.c.	12.54	10.07	840	0.36	1536	0.32
V.a.* vs. *V.m.	12.02	9.81	1138	0.35	1536	0.32
V.a.* vs. *V.p.	11.42	9.79	1380	0.35	1536	0.32
V.a.* vs. *V.v.	12.08	10.06	1138	0.40	747	0.31
V.c.* vs. *V.m.	11.48	9.33	837	0.37	1536	0.32
V.c.* vs. *V.p.	12.63	10.08	748	0.37	747	0.42
V.c.* vs. *V.v.	11.82	9.61	840	0.36	777	0.32
V.m.* vs. *V.p.	12.25	9.88	748	0.38	747	0.41
V.m.* vs. *V.v.	11.29	9.41	1382	0.35	693	0.31
V.p.* vs. *V.v.	12.40	10.14	751	0.44	747	0.44

V.a. = V. alginolyticus, *V.c. = V. cholerae*, *V.m. = V. mimicus*, *V.p. = V. parahaemolyticus* & *V.v. = V. vulnificus*

Support vector machine

The SVM model was based on a 5-class problem. A three-dimensional scatterplot showing 3 out of 10 decision values was generated and visualised from two perspectives (Figure 21). In the right graph (Figure 21B) the decision value between *V. cholerae* and *V. mimicus* emerge as a gap between the bright blue and bright green dots.

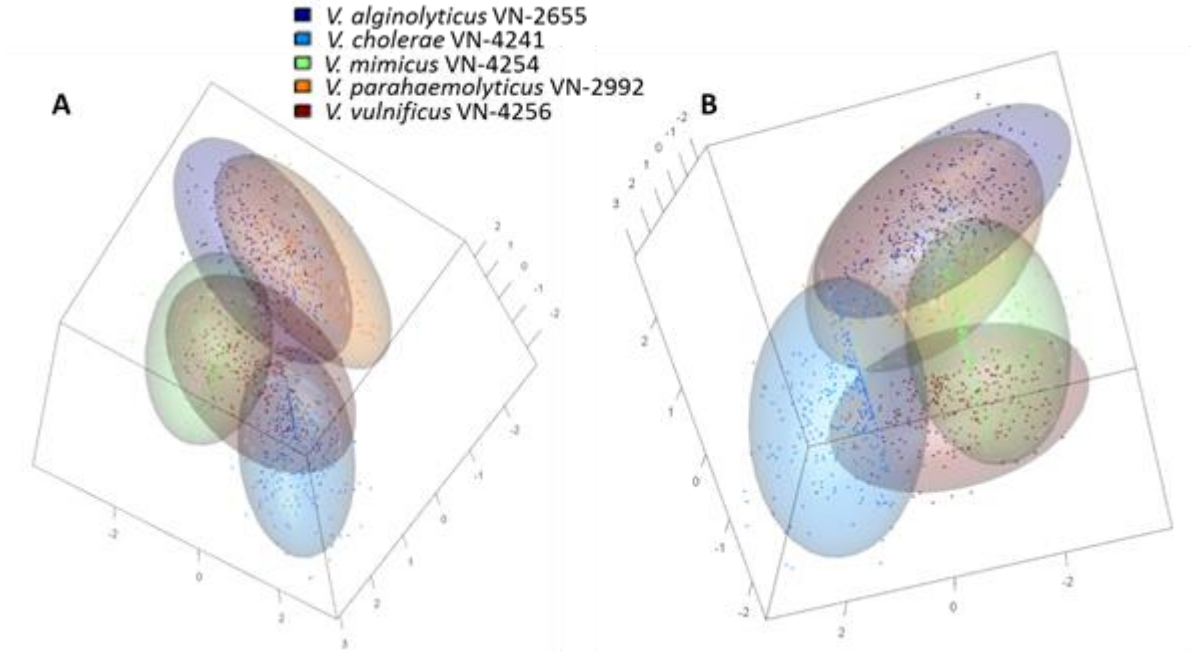

Figure 21: 3D-Scatterplot of SVM model. Surfaces of the ellipses represent 95 % of the confidence level of the total confidence region. 3 out of 10 decision values are plotted. Plot (A) and (B) show different rotations.

The highest concentration of single spectra accumulated at the class borders. Although all species clustered close together, *V. alginolyticus* and *V. parahaemolyticus* seemed to be closer to each other than to the other three species. This observation was proven in the cross-validation of the SVM model which was performed using all 1255 acquired spectra (Table 11).

Table 11 Confusion table of the SVM after a cross-validation. The SVM was tested using all acquired 1255 spectra and an overall accuracy of 88.4 % was achieved.

	Classification result					**Total (1255)**	**Sensitivity [%]**	**Specificity [%]**
	V. a.	***V. c.***	***V. m.***	***V. p.***	***V. v.***			
V. alginolyticus	210	1	6	22	2	241	87.1	95
V. cholerae	4	249	18	3	4	278	89.6	97
V. mimicus	7	15	229	1	5	257	89.1	97
V. parahaemolyticus	31	1	0	219	1	252	86.9	97
V. vulnificus	5	8	10	2	202	227	89.0	98
							Accuracy [%]	**88.4**

An overall accuracy of 88.4 % (spectra classified correctly divided by all items classified) was achieved in the cross-validation. The species-wise sensitivities ranged from 86.9 % (*V. parahaemolyticus*) to 89.6 % (*V. cholerae*). The majority of *V. alginolyticus* spectra were

classified as the right species (210/241, 87.1 % sensitivity) and, while small numbers of spectra were misclassified as *V. cholerae* (1/241, 0.4 %), *V. mimicus* (6/241, 2.5 %) or *V. vulnificus* (2/241, 0.8 %), the biggest number was misclassified as *V. parahaemolyticus* (22/241, 9.1 %). Out of 252 *V. parahaemolyticus* spectra 219 were classified correctly (86.9 %) while the biggest number of wrongly assigned spectra were classified as *V. alginolyticus* (31/252, 12.3 %). Only 2 out of 252 were classified as *V. cholerae* (1/252, 0.4 %) or *V. vulnificus* (1/252, 0.4 %) and none was mistaken as *V. mimicus* (0/252, 0 %). *V. cholerae* spectra were classified correctly with the highest sensitivity of all species (249/278, 89.6 %) and again one species dominated the others in the mismatches. More spectra were assigned to *V. mimicus* (18/241, 6.5 %) than to the species *V. alginolyticus* (4/278, 1.4 %), *V. vulnificus* (4/278, 1.4 %) or *V. parahaemolyticus* (3/278, 1.1 %). Vice versa the *V. mimicus* (229/257, 89.1 %) spectra were more often misclassified as *V. cholerae* (15/257, 5.8 %) than as *V. alginolyticus* (7/257, 2.7 %), V. vulnificus (8/257, 1.9 %) or *V. parahaemolyticus* (1/257, 0.4 %). For *V. vulnificus* (202/227, 89.0 %) the situation was different, because there was more than one species dominating the mismatches. More spectra were wrongly classified to *V. mimicus* (10/227, 4.4 %) or *V. cholerae* (8/227, 3.5 %) than to *V. alginolyticus* (5/227, 2.2 %). The least were assigned to *V. parahaemolyticus* (2/227, 0.9 %).

The five analysed species can be clustered into metagroups due to their genetic relations. *V. alginolyticus* and *V. parahaemolyticus* were joined as group 1, *V. cholerae* and *V. mimicus* as group 2, leaving *V. vulnificus* for group 3. On this level, 98 % of *V. alginolyticus* and *V. parahaemolyticus* as well as 96 % of *V. cholerae* and *V. mimicus* were assigned to the correct groups. As *V. vulnificus* has no other *Vibrio* in its group, the sensitivity does not change between group and species level (Figure 22).

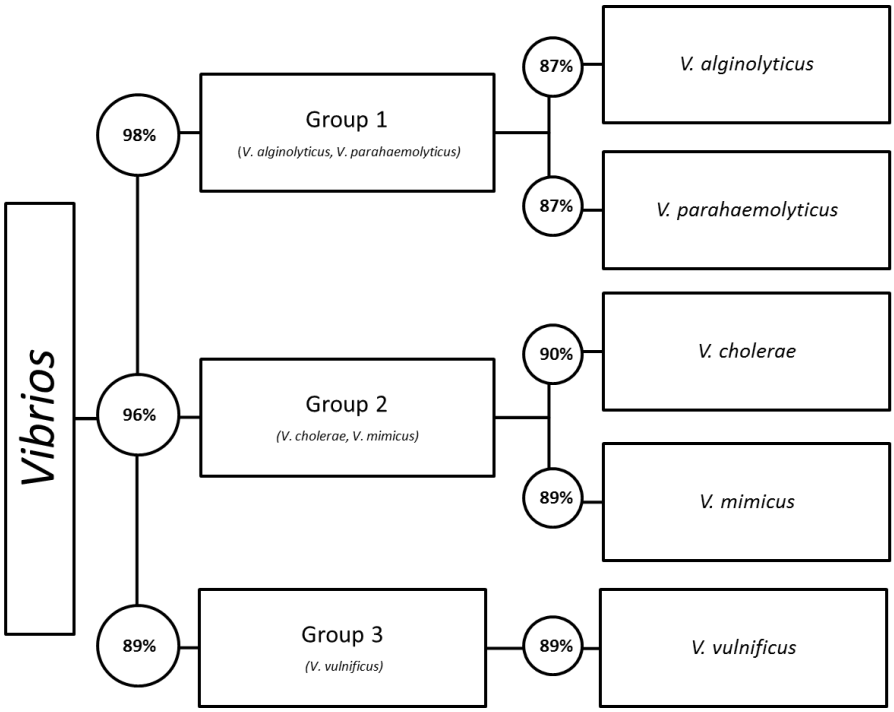

Figure 22: Cross-validation of the SVM. The metagroups were formed due to the genetic relations of the different species. The sensitivity of three meta groups was subsequently calculated using the species level results.

4. Discussion

4.1. Bacterial strains and cultivation

The *Vibrio* spp. used in this work showed differences in growth, which was observed photometrically (OD_{600nm}) after a standardized cultivation in alkaline peptone water. *V. parahaemolyticus* was the fastest growing species, with 1.39 $x10^9$ cells/mL after the incubation for 17 h at 37°C, while the other species *V. alginolyticus* and *V. vulnificus* grew 19 %, *V. cholerae* 30 % and *V. mimicus* 31 % slower than that. It should be considered that the differences in growth, that were seen in the pure cultures, might vary in complex mixed cultures as the species might interact in unknown ways and compete for nutrients. Changes in cultivation conditions have been proven to influence Raman spectra of bacteria before (Harz et al., 2005). As the pre-cultivation of environmental *Vibrio* spp. is still a requirement when analysing sea water samples, these variations should be considered in reference spectra for a correct identification.

4.2. Fluorescence microscopy

Cell concentration determination

The best cell distribution was achieved with cell suspensions containing $5x10^6$ cells/mL on 0.2 µm GTTP filters. Although some cells clustered at the edges of the filtration area, the overall cell distribution was as desired. The calculated optimal cell number of approx. $1x10^4$ cells/mm² can be used to calculate cell concentrations to use on filters with other diameters.

Fluorescent dyes for Raman spectroscopy

CFDA-SE is a vital stain, that needs to be cleaved by intracellular esterases to develop a fluorescence signal. While only insufficient staining was achieved for *V. alginolyticus*, the positive control *E. coli* was stained consistently. As the *Vibrio* cells showed very weak fluorescence signals, the incubation time of 45 min might have been too short. Prolonging the incubation time might solve the problem of insufficient staining, but would counteract the aim of a fast sample preparation. Krause et al. (2007) used CDFA-SE for the investigation of single bacterial cells of different *Bacillus* and *Staphylococcus* spp. in micro-Raman approaches. These gram-positive bacteria were sufficiently stained with CFDA-SE. It has been indicated by Rasmussen et al. (2008), that, although CFDA-SE has the capacity of easily staining gram-positive cells, not all gram-negative bacteria can be stained well. Although it is unclear whether CDFA-SE was hindered from diffusing into the gram-negative *V. alginolyticus* cells or if the intracellular esterase were incapable of cleaving the substrate, the incapacity of CFDA-SE to stain this *Vibrio* disqualified it from further analyses.

The other tested fluorescent dye (SYTO 9) achieved a consistent staining of *V. alginolyticus*. The cells could be detected as particles in the BPE. It is unclear whether the fluorescence signals recorded inside the “tubs” of the nickel slit filter came from residual dye or cells lying inside the “tubs”. Due to the use of dark field microscopic contrasting, the potential effects of

SYTO 9 on the spectra were not determined in the characterization experiments of this study. Krause et al. (2008) demonstrated the importance of the right choice of a fluorescent dye. SYTO 9, which has only little influence on the Raman spectra of e.g. *Bacillus* spp. or *Staphylococcus* spp., is often used in LIVE/DEAD staining together with propidium iodide (PI). While SYTO 9 can easily diffuse through intact cell membranes, PI can only pass perforated membranes and, therefore, can only stain dead cells. When PI intercalated into the DNA of living cells, its excitation maximum shifts to 528 nm which enables the excitation of the fluorochrome by a 532 nm laser. As a consequence, the strong fluorescence signal of PI masks the Raman information. Therefore, the identification of an unknown can not be achieved (Krause et al., 2008).

4.3. Metal array

Only very little cell material is required for micro-Raman spectroscopy and the idea behind the metal array was to increase the efficiency, by optimally utilizing the available space on the relatively expensive metal filters. The tested form of the array was unsuitable for this aim, as the transfer of cells to the filter was insufficient. The best results were achieved by using the array upside down, suggesting that the holes should open up on the filter facing side for future approaches. To enable a complete transfer of cells, the diameter of the holes should be increased.

4.4. Nickel slit filters and silver membrane filters

Due to their structure, the nickel slit filters as well as the silver membrane filters were unsuited for automatic measurements in dark field mode and for quantitative issues. While the “tubs” of the nickel filters caused loss of cells, the granular structure of the silver membrane filters interfered with the cell recognition in fluorescence mode. In addition to the problems of cell detection, the nickel slit filters were not practicable for the qualitative characterization of the *Vibrio* spp. as it was not possible to generate filters with a reproducible distribution of cells.

4.5. Nickel foil

The nickel foil was well suited for the qualitative analysis of pure cultures. It was important to properly wash the cells before spotting them onto foil, to hinder residual media components, among others, from salt crystal formation. A fluent removal of the drops improves the even distribution of cells.

4.6. Particle recognition and automatic selection

The threshold of 225, which was established on the model of *V. alginolyticus* could be conveyed on the other *Vibrio* species. Therefore, it stands to reason, that this threshold can be implemented for characterizations of further *Vibrios*. The morphological variations within the genus *Vibrio* require the adaption of selection criteria. By comparing the five analysed species, two size and elongation ranges were determined for a successful selection. As environmental samples may contain a mixture of cells in different sizes, the set parameters

for selection need to include all the variations, by defining overlapping ranges. This, however, raises the problem of including cell clusters to the analysis.

4.7. Identification of different *Vibrio* spp. via Raman spectroscopy

In the last years, more and more studies focusing on the identification of medically relevant microorganisms by means of Raman spectroscopy have been performed. Organisms of investigation were *Escherichia coli, Pseudomonas spp.*, *Klebsiella pneumoniae*, *Bacillus spp.*, *Staphylococcus spp.* and *Listeria spp.*, to name but a few (Meisel et al., 2014; Kusic et al., 2015; Silge et al., 2014; Stöckel et al., 2009). Although different strains of *V. parahaemolyticus* and *V. vulnificus* have been studied using Raman spectroscopy as well (Xu et al., 2013; Duan et al., 2016; Hlaing et al., 2016), no studies were found targeting identification and differentiation of these potentially pathogenic bacteria on species level. In this thesis, five potentially pathogenic *Vibrio* were characterized and identified by the means of micro-Raman spectroscopy for the first time. Spectra were obtained in a reproducible quality for all analysed *Vibrio* spp. The Raman intensity of the CH-stretch could be used as indicator for a good signal-to-noise ratio. The differences between the species, seen in the mean spectra, were too small to be discerned by the naked eye. Therefore, computer-aided statistical analyses were imperative. The two-way PERMANOVA main tests showed, that the measurements in batches had no influence on the variances of the species. Consequently, the spectra were reproducible for the *Vibrio* spp. The bands found in all five species (749, 1129, 1310 and 1584 cm^{-1}) might explain some of the differences between the species. These bands were assigned to cytochrome c, which is a protein containing a porphyrin and is required for the electron transport chain (Madigan et al., 2006). Cytochrome c absorbs visible light at about 530 nm and is therefore subject to the effect of photobleaching when using a 532 nm laser (Okada et al., 2012; Rösch et al., 2005). During the SIMPER analysis, some of the wavenumbers (747, 748, 751, and 1138 cm^{-1}) that were found to be the highest contributors to the differences between the species, were found to originate from cytochrome c. Remarkably, that was mostly true for species comparisons where two different laser intensities were used to collect the spectra. From the experiments performed, it cannot be derived with certainty whether the different Raman intensities of these bands arise from differences in the chemical compositions of the bacterial cells or whether it was a consequence of photobleaching effects. It would be recommendable to perform Raman measurements for all species with the same laser intensity to ensure that no effects of bleaching influence the data. As the lower laser intensity was insufficient for the smaller *Vibrio* spp., the intensity of 15.75 mW should be chosen for future work. Alternatively, a complete bleaching of cytochrome c should shed light on this question.

As could be expected from the observation of the spectra, the calculated differences between the species were not big (3.8.2, SIMPER, Table 10). However, the high similarity of the species seemed not to hamper the statistical analyses. The separation of the closely related *Vibrio* spp. is a challenging task, that was already examined with different analytical methods. Investigating the genetic relations showed that members of the genus tend to form clusters due to their close relations. Based on the analysis of their 16S rRNA sequence, the similarity for the species pairs *V. cholerae*/*V. mimicus* and *V. alginolyticus*/*V. parahaemolyticus* were

found to be very high at approx. 99.38 % (Kita-Tsukamoto et al., 1993). The same pattern is reflected when comparing the sequences of the rpoB gene (Tarr et al., 2007), which is, in combination with other genes, frequently used for species identification of *Vibrio* spp. (Oberbeckmann et al., 2011a). MALDI-TOF MS, a technique identifying species via their proteome, has become an often used tool in microbiology. To achieve a reliable resolution of closely related *Vibrio* spp., Dieckmann et al. (2010) defined signatures of SIBIs (species-identifying biomarker ions) while Erler et al. (2015) implemented an extensive database (VibrioBase) including over 900 different main spectra. The necessity of this was shown by the observation that one of the chosen strains (VN-4234), in this study identified as *V. mimicus*, was formerly misclassified as *V. cholerae* before the finalized version of the VibrioBase database was established. This shows, that a sufficiently extensive database is necessary for a reliable identification of closely related species via MALDI-TOF MS. Therefore, it stands to reason, that the same problems might occur and be solved in Raman spectroscopy in analogous ways to MALDI-TOF MS.

During this thesis, the same relation patterns between the target species were witnessed at different stages of the analysis. In the one-way PERMANOVA pair-wise tests of the CH-stretch, the results for the comparison of *V. cholerae* and *V. mimicus* ("BPE" data set) indicated, that these two species cannot be differentiated in this spectral region. In contrast, the two species had a significant variance in the CH-stretch within the "Jena" data set, although the evidence against the null hypothesis was not strong either. The loss in resolution that was observed during the "BPE pre-processing" seemed to have a negative influence on the very subtle differences in the CH-stretch region. All pair-wise comparisons of the fingerprint region showed highly significant differences. In the cluster analysis, *V. alginolyticus* and *V. parahaemolyticus* formed a group clearly separated from the other three species. *V. vulnificus* clustered closer to *V. cholerae* and *V. mimicus*, which exhibited the same heterogeneity as *V. alginolyticus* and *V. parahaemolyticus*. The distances between the species were higher, when comparing the fingerprint region than in the CH-stretch region, which is another hint that more interspecies differences are explained in this region. From the observations in the pair-wise comparisons, the cluster analysis and the fact that the fingerprint region contributes more to the variations between the species, it can be concluded that the fingerprint region is sufficient for the identification of *Vibrio* spp. Beyond that, the CH-stretch region might even interfere with the distinguishability of closely related species.

Also, in the cross-validation of the SVM, most misclassifications happened between the closely related *Vibrio* spp. Although the five species clustered close together, as could be seen in the 3D-scatterplot (Figure 21), the SVM was still able to classify most spectra correctly. This shows the high potential of this machine learning programme to identify even closely related species. The data set used for the SVM-training was relatively small and an expansion of it might further improve the differentiation and identification of the *Vibrio* spp. The more spectra are included in finding the class boarders and creating the decision values, the more reliable the model of the SVM is.

5. Outlook

To be able to investigate the environmental *Vibrio* population, some questions still need to be answered and hurdles have to be overcome. As many other pathogens, *Vibrio* spp. are known to enter a viable but not cultivatable (VBNC) state when they are facing unfavourable environmental conditions (Thompson et al., 2004). Conventional microbiological cultivation methods and identification methods based on pre-cultivations fail to detect and identify microorganisms in this state. With its potential to identify bacteria on single cell level, micro-Raman spectroscopy appears as a promising method. To be able to detect single cells in environmental water samples and to answer quantitative issues, another way of sample preparation needs to be found. Pahlow et al. (2016) presented a siderophore based isolation and enrichment strategy for *Pseudomonas* spp.. Aluminium chips loaded with immobilized siderophore iron complexes were used to specifically capture *Pseudomonas* spp. from spiked tab water samples and identify them via Raman spectroscopy. The identification results of the fully trained SVM classifier had average sensitivities of 85.99 % and an overall accuracy of 85.5 % for five different *Pseudomonas* spp.. Siderophores are used by microorganisms to scavenge nutritional iron from their environment. These proteins are known to be expressed by *Vibrio* spp. (León-Sicairos et al., 2015; Griffiths et al., 1984; Okujo et al., 1994) and might, therefore, be a starting point for a specific isolation and enrichment strategy for environmental *Vibrio* spp.. In order to be able to identify unknown *Vibrio* spp. in environmental samples, reference spectra need to be provided. The results from the statistics established two different ways of identification, either by correlating unknown spectra to a database or feeding them to a fully trained SVM classifier. Considering, that Raman spectra are metabolic snapshots of cells, differences caused by cultivation conditions or variances appearing during the different stages of a lifecycle need to be taken into account. Therefore, an extensive collection of spectra must be created for both approaches.

In conclusion, it can be said, that due to the easy handling, the fast sample preparation, the high information yield and the requirement of very little sample material, Raman spectroscopy is a promising tool for the identification of potentially pathogenic *Vibrio* spp.. The precondition for this is that the difficulties unveiled in this thesis can be overcome.

Acknowledgement

I would like to express my gratitude to everyone who walked with me along the way of this thesis. Thanks to Dr. Gunnar Gerdts and Dr. Antje Wichels whose supervision and support has been of enormous value and enabled me to grow with this work. Thank you for giving me the opportunity to be a part of your team at the “Biologische Anstalt Helgoland”.

Special thanks to my cooperation partners at the Friedrich-Schiller-University (Helmholtzweg 4, 07743 Jena, Germany) for their excellent help. Dr. Anja Silge supported me in many ways with her knowledge and various good tips about handling the “BPE” and how to further improve my spectra. Together with Priv.-Doz. Dr. rer. nat. Thomas Bocklitz, she was responsible for the “Jena” data pre-processing and support vector machine, which became a particularly important part of my thesis.

I want to thank Prof. Dr. Harald Pichler for his supervision and for backing me and my decision to conduct my thesis abroad.

“Thank you!” to my wonderful mentor Sidika Hackbusch, who has always been there for me with competent advice and support whenever I needed guidance. It was a great time on Helgoland with all you “Micros”, “Bios” and all the other wonderful people I got to meet on the island. I want to thank you for the happy times, the talks and the walks we shared.

I want to thank my family for their unconditional support and for being by my side wherever I go. And finally, and without hesitation, I wish to thank Christian Seelich, for all the times he lent me his ear and encouraged me to believe in myself.

I. Literature

AUSTIN, B. 2010. Vibrios as causal agents of zoonoses. *Veterinary Microbiology,* 140**,** 310-7.

BAKER-AUSTIN, C., STOCKLEY, L., RANGDALE, R., et al. 2010. Environmental occurrence and clinical impact of Vibrio vulnificus and Vibrio parahaemolyticus: a European perspective. *Environ Microbiol Rep,* 2**,** 7-18.

BAKER-AUSTIN, C., TRINANES, J., TAYLOR, N. G. H., et al. 2012. Emerging Vibrio risk at high latitudes in response to ocean warming. *Nature Clim. Change,* 3**,** 73-7.

BARBIERI, E., FALZANO, L., FIORENTINI, C., et al. 1999. Occurrence, Diversity, and Pathogenicity of Halophilic Vibrio spp. and Non-O1 Vibrio cholerae from Estuarine Waters along the Italian Adriatic Coast. *Applied and Environmental Microbiology,* 65**,** 2748-53.

BOCKLITZ, T., WALTER, A., HARTMANN, K., et al. 2011. How to pre-process Raman spectra for reliable and stable models? *Analytica Chimica Acta,* 704**,** 47-56.

CHAN, J. W., WINHOLD, H., CORZETT, M. H., et al. 2007. Monitoring dynamic protein expression in living E. coli. Bacterial cells by laser tweezers Raman spectroscopy. *Cytometry A,* 71**,** 468-74.

DIECKMANN, R., STRAUCH, E. & ALTER, T. 2010. Rapid identification and characterization of Vibrio species using whole-cell MALDI-TOF mass spectrometry. *Journal of applied microbiology,* 109**,** 199-211.

DÖRFER, T., BOCKLITZ, T., TARCEA, N., et al. 2011. Checking and improving calibration of Raman spectra using chemometric approaches. *Zeitschrift für Physikalische Chemie International journal of research in physical chemistry and chemical physics,* 225**,** 753-64.

DUAN, N., YAN, Y., WU, S., et al. 2016. Vibrio parahaemolyticus detection aptasensor using surface-enhanced Raman scattering. *Food Control,* 63**,** 122-7.

EILER, A., JOHANSSON, M. & BERTILSSON, S. 2006. Environmental influences on Vibrio populations in northern temperate and boreal coastal waters (Baltic and Skagerrak Seas). *Applied and Environmental Microbiology,* 72**,** 6004-11.

ERLER, R., WICHELS, A., HEINEMEYER, E. A., et al. 2015. VibrioBase: A MALDI-TOF MS database for fast identification of Vibrio spp. that are potentially pathogenic in humans. *Syst Appl Microbiol,* 38**,** 16-25.

FARMER, J. J. I., JANDA, J. M., BRENNER, F. W., et al. 2005. Order XI. "Vibrionales". *In:* GARRITY, G. M., BRENNER, D. J., KRIEG, N. R., et al. (eds.) *Bergey's Manual® of Systematic Bacteriology Volume 2: The Proteobacteria, Part B: The Gammaproteobacteria.* East Lansing, USA: Springer US.

GRIFFITHS, G., SIGEL, S., PAYNE, S., et al. 1984. Vibriobactin, a siderophore from Vibrio cholerae. *Journal of Biological Chemistry,* 259**,** 383-5.

HARZ, M., ROSCH, P., PESCHKE, K. D., et al. 2005. Micro-Raman spectroscopic identification of bacterial cells of the genus Staphylococcus and dependence on their cultivation conditions. *Analyst,* 130**,** 1543-50.

HARZ, M., RÖSCH, P. & POPP, J. 2009. Vibrational spectroscopy—A powerful tool for the rapid identification of microbial cells at the single-cell level. *Cytometry Part A,* 75**,** 104-13.

HLAING, M. M., DUNN, M., STODDART, P. R., et al. 2016. Raman spectroscopic identification of single bacterial cells at different stages of their lifecycle. *Vibrational Spectroscopy,* 86**,** 81-9.

HOLLAS, J. M. 2004. *Modern Spectroscopy, 4th Edition*.

HORNSTRUP, M. K. & GAHRN-HANSEN, B. 1993. Extraintestinal infections caused by Vibrio parahaemolyticus and Vibrio alginolyticus in a Danish county, 1987–1992. *Scandinavian journal of infectious diseases,* 25**,** 735-40.

HUANG, W. E., GRIFFITHS, R. I., THOMPSON, I. P., et al. 2004. Raman microscopic analysis of single microbial cells. *Analytical Chemistry,* 76**,** 4452-8.

KIRSTEIN, I. V., KIRMIZI, S., WICHELS, A., et al. 2016. Dangerous hitchhikers? Evidence for potentially pathogenic Vibrio spp. on microplastic particles. *Mar Environ Res,* 120**,** 1-8.

KITA-TSUKAMOTO, K., OYAIZU, H., NANBA, K., et al. 1993. Phylogenetic relationships of marine bacteria, mainly members of the family Vibrionaceae, determined on the basis of 16S rRNA sequences. *International Journal of Systematic and Evolutionary Microbiology,* 43**,** 8-19.

KRAUSE, M., RADT, B., RÖSCH, P., et al. 2007. The investigation of single bacteria by means of fluorescence staining and Raman spectroscopy. *Journal of Raman Spectroscopy,* 38**,** 369-72.

KRAUSE, M., RÖSCH, P., RADT, B., et al. 2008. Localizing and Identifying Living Bacteria in an Abiotic Environment by a Combination of Raman and Fluorescence Microscopy. *Analytical Chemistry,* 80**,** 8.

KUSIC, D., KAMPE, B., RAMOJI, A., et al. 2015. Raman spectroscopic differentiation of planktonic bacteria and biofilms. *Anal Bioanal Chem,* 407**,** 6803-13.

LAMBERT, J. B., MARSMANN, H., GRONERT, S., et al. 2012. *Spektroskopie - Strukturaufklärung in der Organischen Chemie*, Pearson, Higher Education.

LEÓN-SICAIROS, N., ANGULO-ZAMUDIO, U. A., DE LA GARZA, M., et al. 2015. Strategies of Vibrio parahaemolyticus to acquire nutritional iron during host colonization. *Frontiers in microbiology,* 6.

LONG, D. A. 2002. *The Raman effect : a unified treatment of the theory of Raman scattering by molecules,* Chichester, John Wiley & Sons Ltd.

MADIGAN, M. T., MARTINKO, J. M. & BROCK, T. D. 2006. *Brock Mikrobiologie*, Pearson Deutschland GmbH.

MAQUELIN, K., KIRSCHNER, C., CHOO-SMITH, L. P., et al. 2002. Identification of medically relevant microorganisms by vibrational spectroscopy. *Journal of Microbiological Methods,* 51**,** 255-71.

MARTINEZ-URTAZA, J., SIMENTAL, L., VELASCO, D., et al. 2005. Pandemic Vibrio parahaemolyticus O3:K6, Europe. *Emerg Infect Dis,* 11**,** 1319-20.

MEISEL, S., STOCKEL, S., ROSCH, P., et al. 2014. Identification of meat-associated pathogens via Raman microspectroscopy. *Food Microbiol,* 38**,** 36-43.

OBERBECKMANN, S., WICHELS, A., MAIER, T., et al. 2011a. A polyphasic approach for the differentiation of environmental Vibrio isolates from temperate waters. *FEMS Microbiol Ecol,* 75**,** 145-62.

OBERBECKMANN, S., WICHELS, A., WILTSHIRE, K. H., et al. 2011b. Occurrence of Vibrio parahaemolyticus and Vibrio alginolyticus in the German Bight over a seasonal cycle. *Antonie Van Leeuwenhoek,* 100**,** 291-307.

OKADA, M., SMITH, N. I., PALONPON, A. F., et al. 2012. Label-free Raman observation of cytochrome c dynamics during apoptosis. *Proceedings of the National Academy of Sciences,* 109**,** 28-32.

OKUJO, N., SAITO, M., YAMAMOTO, S., et al. 1994. Structure of vulnibactin, a new polyamine-containing siderophore from Vibrio vulnificus. *Biometals,* 7**,** 109-16.

OPPENHEIMER, C. H. & ZOBELL, C. E. 1952. The growth an viability of sixty three species of marine bacteria influenced by hydrostatic pressure. *Journal of Marine Research,* 11**,** 10-8.

OTTO, M. 2006. *Analytische Chemie,* Weinheim, John Wiley & Sons.

PAHLOW, S., STOCKEL, S., POLLOK, S., et al. 2016. Rapid Identification of Pseudomonas spp. via Raman Spectroscopy Using Pyoverdine as Capture Probe. *Analytical Chemistry,* 88**,** 1570-7.

PATEL, A., NOBLE, R. T., STEELE, J. A., et al. 2007. Virus and prokaryote enumeration from planktonic aquatic environments by epifluorescence microscopy with SYBR Green I. *Nat Protoc,* 2**,** 269-76.

RAMAN, C. V. & KRISHNAN, K. S. 1928. A new type of secundary radiation. *Nature,* 121**,** 501-2.

RASBAND, W. S. 1997-2016. ImageJ. U. S. National Institutes of Health, Bethesda, Maryland, USA.

RASMUSSEN, M. B., ODDERSHEDE, L. B. & SIEGUMFELDT, H. 2008. Optical tweezers cause physiological damage to Escherichia coli and Listeria bacteria. *Applied and environmental microbiology,* 74**,** 2441-6.

READ, D. S. & WHITELEY, A. S. 2015. Chemical fixation methods for Raman spectroscopy-based analysis of bacteria. *Journal of Microbiological Methods,* 109**,** 79-83.

RÖSCH, P., HARZ, M., SCHMITT, M., et al. 2005. Chemotaxonomic identification of single bacteria by micro-Raman spectroscopy: application to clean-room-relevant biological contaminations. *Applied and environmental microbiology,* 71**,** 1626-37.

ROTTENFUSSER, R., WILSON, E. E. & DAVIDSON, M. W. 2014. Education in Microscopy and Digital Imaging. *ZEISS Microscopy*.

RYAN, C., CLAYTON, E., GRIFFIN, W., et al. 1988. SNIP, a statistics-sensitive background treatment for the quantitative analysis of PIXE spectra in geoscience applications. *Nuclear Instruments and Methods in Physics Research Section B: Beam Interactions with Materials and Atoms,* 34**,** 396-402.

SILGE, A., SCHUMACHER, W., ROSCH, P., et al. 2014. Identification of water-conditioned Pseudomonas aeruginosa by Raman microspectroscopy on a single cell level. *Syst Appl Microbiol,* 37**,** 360-7.

SMEKAL, A. 1923. Zur Quantentheorie der Dispersion. *Die Naturwissenschaft,* 43.

SMITH, E. & DENT, G. 2005. *Modern Raman spectroscopy: a practical approach,* Chichester, John Wiley & Sons Ltd.

STÖCKEL, S., KIRCHHOFF, J., NEUGEBAUER, U., et al. 2016. The application of Raman spectroscopy for the detection and identification of microorganisms. *Journal of Raman Spectroscopy,* 47**,** 89-109.

STÖCKEL, S., MEISEL, S., BÖHME, R., et al. 2009. Effect of supplementary manganese on the sporulation ofBacillusendospores analysed by Raman spectroscopy. *Journal of Raman Spectroscopy,* 40**,** 1469-77.

TAKAHASHI, A., MIYOSHI, S. I., TAKATA, N., et al. 2007. Haemolysin produced by Vibrio mimicus activates two Cl–secretory pathways in cultured intestinal-like Caco-2 cells. *Cellular microbiology,* 9**,** 583-95.

TARR, C. L., PATEL, J. S., PUHR, N. D., et al. 2007. Identification of Vibrio isolates by a multiplex PCR assay and rpoB sequence determination. *Journal of clinical microbiology,* 45**,** 134-40.

THOMPSON, F. L., IIDA, T. & SWINGS, J. 2004. Biodiversity of vibrios. *Microbiol Mol Biol Rev,* 68**,** 403-31.

WILLIAMS, A. C. & EDWARDS, H. G. M. 1994. Fourier Transform Raman Spectroscopy of Bacterial Cell Walls. 673-7.

XU, J., TURNER, J. W., IDSO, M., et al. 2013. In situ strain-level detection and identification of Vibrio parahaemolyticus using surface-enhanced Raman spectroscopy. *Analytical chemistry,* 85**,** 2630-7.

II. List of figures

III. List of tables

IV. Abbreviations

APW	alkaline peptone water
df	degrees of freedom
DNA	Desoxyribonucleic acid
FT-IR	Fourier transform infrared spectroscopy
GS/s	gigasamples per second
H_2O	water
IR	Infrared
m/z	Mass to charge ratio in Mass spectrogram
MALDI-TOF	Matrix Assisted Laser Desorption/Ionization – Time of Flight
MS	Mass Spectrometry
MB-50%	Marine broth agar, 50% reduced salinity
MQW	Ultrapure water
MS	mean square
rpm	revolutions per minute
rRNA	ribosomal Ribonucleic acid
SD	Standard deviation
spp.	species (plural)
SS	sum of squares
V.	*Vibrio*
V.a.	*V. alginolyticus*
V.c.	*V. cholerae*
V.m.	*V. mimicus*
V.p.	*V. parahaemolyticus*
V.v.	*V. vulnificus*
VN	VibrioNet
x	times